

NASA/TM—2000-210239



Body-Vortex Interaction, Sound Generation and Destructive Interference

Hsiao C. Kao
Glenn Research Center, Cleveland, Ohio

August 2000

The NASA STI Program Office . . . in Profile

Since its founding, NASA has been dedicated to the advancement of aeronautics and space science. The NASA Scientific and Technical Information (STI) Program Office plays a key part in helping NASA maintain this important role.

The NASA STI Program Office is operated by Langley Research Center, the Lead Center for NASA's scientific and technical information. The NASA STI Program Office provides access to the NASA STI Database, the largest collection of aeronautical and space science STI in the world. The Program Office is also NASA's institutional mechanism for disseminating the results of its research and development activities. These results are published by NASA in the NASA STI Report Series, which includes the following report types:

- **TECHNICAL PUBLICATION.** Reports of completed research or a major significant phase of research that present the results of NASA programs and include extensive data or theoretical analysis. Includes compilations of significant scientific and technical data and information deemed to be of continuing reference value. NASA's counterpart of peer-reviewed formal professional papers but has less stringent limitations on manuscript length and extent of graphic presentations.
- **TECHNICAL MEMORANDUM.** Scientific and technical findings that are preliminary or of specialized interest, e.g., quick release reports, working papers, and bibliographies that contain minimal annotation. Does not contain extensive analysis.
- **CONTRACTOR REPORT.** Scientific and technical findings by NASA-sponsored contractors and grantees.

- **CONFERENCE PUBLICATION.** Collected papers from scientific and technical conferences, symposia, seminars, or other meetings sponsored or cosponsored by NASA.
- **SPECIAL PUBLICATION.** Scientific, technical, or historical information from NASA programs, projects, and missions, often concerned with subjects having substantial public interest.
- **TECHNICAL TRANSLATION.** English-language translations of foreign scientific and technical material pertinent to NASA's mission.

Specialized services that complement the STI Program Office's diverse offerings include creating custom thesauri, building customized data bases, organizing and publishing research results . . . even providing videos.

For more information about the NASA STI Program Office, see the following:

- Access the NASA STI Program Home Page at <http://www.sti.nasa.gov>
- E-mail your question via the Internet to help@sti.nasa.gov
- Fax your question to the NASA Access Help Desk at (301) 621-0134
- Telephone the NASA Access Help Desk at (301) 621-0390
- Write to:
NASA Access Help Desk
NASA Center for Aerospace Information
7121 Standard Drive
Hanover, MD 21076

NASA/TM—2000-210239



Body-Vortex Interaction, Sound Generation and Destructive Interference

Hsiao C. Kao
Glenn Research Center, Cleveland, Ohio

National Aeronautics and
Space Administration

Glenn Research Center

August 2000

This report contains preliminary findings, subject to revision as analysis proceeds.

Available from

NASA Center for Aerospace Information
7121 Standard Drive
Hanover, MD 21076
Price Code: A03

National Technical Information Service
5285 Port Royal Road
Springfield, VA 22100
Price Code: A03

BODY-VORTEX INTERACTION, SOUND GENERATION AND DESTRUCTIVE INTERFERENCE

Hsiao C. Kao
National Aeronautics and Astronautics Administration
Glenn Research Center
Cleveland, Ohio 44135

ABSTRACT

It is generally recognized that interaction of vortices with downstream blades is a major source of noise production. To analyze this problem numerically, a two-dimensional model of inviscid flow together with the method of matched asymptotic expansions is proposed. The method of matched asymptotic expansions is used to match the inner region of incompressible flow to the outer region of compressible flow. Because of incompressibility, relatively simple numerical methods are available to treat multiple vortices and multiple bodies of arbitrary shape. Disturbances from vortices and bodies propagate outward as sound waves. Due to their interactions, either constructive or destructive interference may result. When it is destructive, the combined sound intensity can be reduced, sometimes substantially. In addition, an analytical solution to sound generation by the cascade-vortex interaction is given.

1. INTRODUCTION

Interaction of rotor tip vortices with downstream stators or other blades is commonly regarded as an important source of noise production (Refs. 1-3). Although it is difficult to separate vortices from other secondary flow effects, the notion that vortices play an important role is generally accepted. In order to make the problem tractable, a two-dimensional model with rectilinear vortices in an inviscid flow is proposed. The cases to be considered are: a moving vortex interacting with a single body (blade) and with several bodies, several moving vortices interacting with several bodies, and vortices interacting with a cascade. Since the unsteady Kutta condition will be imposed, wakes behind the blades are expected to occur.

The main assumption made here is that the bodies must be acoustically compact. In other words, the Mach number must be relatively low. This enables us to use the method of asymptotic expansions to match the inner solution, which is incompressible, with the outer solution, which is compressible and satisfies the acoustic equation. Since several bodies may be present, both constructive and destructive interference of sound waves from neighboring bodies have to be considered. By manipulating the interference, it is possible to achieve pressure attenuation and reduce sound intensity.

Under the assumption of low Mach number, the characteristic length of the body is in general much smaller than the acoustic wave length, which implies that the compactness ratio is small and the flow in the vicinity of the body is not wave like. Dowling and

Ffowcs Williams (Ref. 4, p.40) stated that all acoustic motions in the vicinity of a singularity are solutions of Laplace's equations. In the present investigation a body is represented by surface vorticity elements. Therefore, the inner region surrounding the body is incompressible and is governed by the Laplace equation. Disturbances generated in this region propagate outward as acoustic signals. Thus, the outer region is compressible and governed by the acoustic equation.

Using asymptotic matching to solve aeroacoustic problems in low-speed flows has been examined previously (Refs. 6-12 for example). In these studies if a body is present, it is usually of simple shape and amenable to conformal mapping. Here this method is broadened to include multiple bodies of arbitrary shape. With this extension, interference of neighboring bodies can be studied.

The time scale for blade-vortex interaction is of the order of \bar{L} / \bar{U}_0 , where \bar{L} is the length of the body and \bar{U}_0 is the freestream velocity. In this time interval an acoustic wave has propagated to the distance of \bar{L} / M_0 , which is much larger than \bar{L} as M_0 , the freestream Mach number, approaches to zero. Thus, there are two disparate lengths, an indication of a singular perturbation problem.

The advantage of this approach lies mostly in the inner region, where incompressible solutions for several bodies can be obtained readily by a number of numerical methods. The method chosen here is Martensen's surface vorticity method. This method, which has been thoroughly investigated by Lewis (Ref. 5), is convenient for the present purpose, since the surface is replaced by vorticity elements, which along with moving vortices can be treated similarly by the Biot-Savart law.

The acoustic equation in the outer region, after the Fourier Transform, becomes a Bessel equation, whose outgoing wave is represented by a Hankel function. Therefore, none of the unresolved complications in computational aeroacoustics appears. The remaining task is to match the two regions and to perform the inverse Fourier transform to return to the physical space.

2. METHOD VALIDATION

In order to gain confidence of using asymptotic matching to solve aeroacoustic problems, a simple problem of acoustic radiation by an oscillating circular cylinder is first examined. It so happens that in this case a term-by-term comparison between the analytical and asymptotic solutions can be made without recourse to numerical results. Although this is a simple example, the matching procedures for more complicated problems are the same. Therefore, more details than necessary are given below in order to lessen explanations for vortex interaction problems later.

2.1 Inner Solution and its Fourier Transform

The motion of an oscillating circular cylinder as depicted in Fig.1 is expressed as $\bar{U}_c \exp(i\bar{\omega}_c \bar{t})$, whose normal component on the surface is $\bar{U}_c \exp(i\bar{\omega}_c \bar{t}) \cos \theta$. Thus the velocity potential is

$$\bar{\phi} = -\bar{U}_c \frac{\bar{a}^2}{\bar{r}} \exp(i\bar{\omega}_c \bar{t}) \cos \theta ,$$

where \bar{U}_c is the amplitude of oscillating velocity, \bar{a} the radius of the cylinder, $\bar{\omega}_c$ the angular frequency, \bar{r} the radial distance, \bar{c} the speed of sound, and \bar{t} the time. For small oscillations, the linearized Bernoulli equation is valid and gives the perturbed pressure in the inner region as

$$p'_i = -\frac{\partial \phi}{\partial t} = \frac{i\omega_c M_c}{R} \cos \theta \exp(i\omega_c t) \quad (1)$$

The symbols in this equation refer to dimensionless quantities and are defined as follows:

$$p'_i = \frac{\bar{p}'}{\bar{\rho}_0 \bar{U}_c^2} \quad \phi = \frac{\bar{\phi}}{\bar{U}_c \bar{a}} \quad \omega_c = \frac{\bar{\omega}_c \bar{a}}{\bar{U}_c} \quad r = \frac{\bar{r}}{\bar{a}} \quad R = M_c r$$

$$M_c = \frac{\bar{U}}{\bar{c}} \quad t = \frac{\bar{t} \bar{U}_c}{\bar{a}}$$

Applying the Fourier transform pair to Eq. (1)

$$\hat{f}(R, \omega) = \int_{-\infty}^{\infty} f(R, t) e^{-i\omega t} dt, \quad f(R, t) = \frac{1}{2\pi} \int_{-\infty}^{\infty} \hat{f}(R, \omega) e^{i\omega t} d\omega \quad (2)$$

to give

$$\hat{p}'_i = \frac{i\omega_c M_c}{R} \cos \theta \int_{-\infty}^{\infty} e^{-i(\omega - \omega_c)t} dt = \frac{i2\pi\omega_c M_c}{R} \cos \theta \delta(\omega - \omega_c), \quad (3)$$

where $\delta(\omega - \omega_c)$ denotes the δ -function (Ref. 13).

2.2 Outer Equation and its Solution

As mentioned previously, there is an outer characteristic length, which is much larger than the body length. This length can now be used to rescale the coordinates in the outer region to give

$$X = M_c \frac{\bar{x}}{\bar{a}}, \quad Y = M_c \frac{\bar{y}}{\bar{a}}$$

With the rescaled coordinates held fixed and letting the Mach number tend to zero, the governing equation reduces to the classical acoustic equation. Its form in polar coordinates becomes

$$\frac{\partial^2 p'_0}{\partial R^2} + \frac{1}{R} \frac{\partial p'_0}{\partial R} + \frac{1}{R^2} \frac{\partial^2 p'_0}{\partial \theta^2} - \frac{\partial^2 p'_0}{\partial t^2} = 0, \quad (4)$$

where the subscript o refers to the perturbed p in the outer region. In view of the inner solution in Eq. (1), the outer solution is assumed to be of the form

$$p'_0 = q_0(R,t) \cos \theta . \quad (5)$$

Upon substitution of this expression in Eq. (4) and applying the Fourier transform, it becomes

$$\frac{d^2 \hat{q}_0}{dR^2} + \frac{1}{R} \frac{d\hat{q}_0}{dR} + (\omega^2 - \frac{1}{R^2}) \hat{q}_0 = 0, \quad (6)$$

This is the Bessel equation of the first order, whose solution for the outgoing wave is the Hankel function of the second kind and is given by

$$\hat{p}'_0 = A H_1^{(2)}(\omega R) \cos \theta , \quad (7)$$

where A is the unknown coefficient to be determined by matching.

2.3 Matching and Inverse Transform

Eq. (7) is to be matched with the inner solution Eq. (3) by the method of asymptotic matching (Ref. 14). With the aid of Ref. 15 for $R \rightarrow 0$, Eq. (7) reduces to

$$\hat{p}'_0 \cong \frac{iA}{\pi} \frac{2}{\omega R} \cos \theta .$$

Comparing this expression with Eq. (3) gives

$$A = \pi^2 M_c \omega_c \omega \delta(\omega - \omega_c)$$

$$\hat{p}'_0 = \pi^2 M_c \omega_c \omega \delta(\omega - \omega_c) H_1^{(2)}(\omega R) \cos \theta . \quad (8)$$

The inverse transform of Eq. (8) is

$$\begin{aligned} p'_0 &= \frac{1}{2\pi} \int_{-\infty}^{\infty} \hat{p}'_0 e^{i\omega t} d\omega = \frac{\pi M_c \omega_c}{2} \cos \theta \int_{-\infty}^{\infty} \omega \delta(\omega - \omega_c) H_1^{(2)}(\omega R) e^{i\omega t} d\omega \\ &= \frac{\pi M_c \omega_c^2}{2} \cos \theta H_1^{(2)}(\omega_c R) e^{i\omega_c t} . \end{aligned} \quad (9)$$

This expression represents the far-field sound pressure radiated from the oscillating cylinder and is equivalent to the analytical solution of Eq. (2-69) in Ref. 4. Since their solution was written with different notation and the present solution is only valid for a

small compactness ratio, $2\pi\bar{a}/\bar{\lambda} = \omega_c M_c \ll 1$, where $\bar{\lambda}$ is the acoustic wavelength, their solution is first cast in the form

$$p'_0 = \frac{-1}{iM_c} \cos\theta e^{i\omega_c t} \frac{H_1^{(2)}(\omega_c R)}{H_0^{\prime(2)}(\omega_c M)} \quad (10)$$

where all quantities have been made dimensionless in accordance to the present notation, and the primes affixed to the Hankel function refer to differentiations. $H_0^{\prime(2)}(\omega r/c)$ in Ref. 4 has been replaced by the Hankel function of the first order $-H_1^{(2)}(\omega_c R)$, and $i\omega\epsilon$ by \bar{U}_c . Under the assumption of a small compactness ratio, the denominator becomes (Ref. 15)

$$H_0^{\prime(2)}(\omega_c M) \cong \frac{-2}{i\pi} \frac{1}{\omega_c^2 M_c^2}$$

With this expression given, one finds that Eq. (10) is equal to Eq. (9). The last step is necessary, because the present method is valid for small compactness ratios.

For this simple example, the Fourier integrals can be determined analytically. For more complicated cases, recourse to numerical methods, such as the discrete Fourier transform in Ref. 13, is necessary. Therefore, an accurate evaluation of Fourier integrals is crucial. In order to demonstrate this, we worked out numerically two Fourier integrals in Ref. 7 and then compared them with Crighton's analytic expressions. The agreement turned out to be rather good. Details of this comparison will be given later.

3. FORMULATION OF PROBLEM IN INNER REGION

Since the flow in the inner region is incompressible, its complex potential is

$$W = \Phi + i\Psi = \sum_{m=1}^M \frac{i\gamma_m ds_m}{2\pi} \log(z - z_m) + \sum_{j=1}^N \frac{i\Gamma_j}{2\pi} \log(z - z_j) + z \quad (11)$$

where $z = x + iy$ represents a field point in the flow field, $z_m = x_m + iy_m$ refers to the mid-point in the surface vorticity element s_m , whose vorticity strength per unit length is γ_m , and ds_m is the length of this element (Fig. 2). The symbol $z_j = x_j + iy_j$ refers to the location of Γ_j . The vorticity strengths γ_m and Γ_j is defined to be positive when clockwise in accordance with Lewis' convention. The first group of terms refers to M surface vorticity elements of unknown strengths and the second group to N free vortices of given strengths. The last term denotes the complex potential of the freestream velocity. All quantities are dimensionless, which are defined in a similar manner as for Eq. (1). The characteristic length here is the longitudinal length of the body \bar{L} , and the characteristic velocity is the freestream velocity \bar{U}_0 .

The derivative of W with respect to z gives the field velocity components u and v in the x - and y -direction as follows:

$$\begin{aligned}
 u(x, y) &= \sum_{m=1}^M \frac{\gamma_m ds_m}{2\pi} \frac{y - y_m}{(x - x_m)^2 + (y - y_m)^2} + \sum_{j=1}^N \frac{\Gamma_j}{2\pi} \frac{y - y_j}{(x - x_j)^2 + (y - y_j)^2} + 1 \\
 v(x, y) &= -\sum_{m=1}^M \frac{\gamma_m ds_m}{2\pi} \frac{x - x_m}{(x - x_m)^2 + (y - y_m)^2} - \sum_{j=1}^N \frac{\Gamma_j}{2\pi} \frac{x - x_j}{(x - x_j)^2 + (y - y_j)^2}
 \end{aligned} \tag{12}$$

The free stream velocity is assumed to be always parallel to the x -direction. Thus, the angle of attack of a body is the angle between the x -axis and the blade chord.

As the field point x and y approaches the surface point x_m and y_m , Eqs. (12) reduce to Eq. (13). The solution of this system determines the unknowns γ_m .

$$\frac{1}{2\pi} \sum_{m=1, m \neq n}^M \gamma_m ds_m K_b(s_n, s_m) + \gamma_n \left(\frac{1}{4\pi} \frac{ds_n}{R_n} - \frac{1}{2} \right) = -\frac{1}{2\pi} \sum_{j=1}^N \Gamma_j K_v(s_n, z_j) - \cos \theta_n$$

where

$$\begin{aligned}
 n &= 1, \dots, M \\
 K_b(s_n, s_m) &= \frac{(y_n - y_m) \cos \theta_n - (x_n - x_m) \sin \theta_n}{(x_n - x_m)^2 + (y_n - y_m)^2} \\
 K_v(s_n, s_j) &= \frac{(y_n - y_j) \cos \theta_n - (x_n - x_j) \sin \theta_n}{(x_n - x_j)^2 + (y_n - y_j)^2}
 \end{aligned} \tag{13}$$

Here $K_b(s_n, s_m)$ and $K_v(s_n, s_j)$ are two influence coefficients representing the tangential velocity components at s_n induced by other vorticity elements and by free vortices respectively. The symbol R_n is the radius of curvature at s_n and θ_n the tangential angle (Fig. 2). The second term in the first equation accounts for the self-induced velocity of γ_n at element s_n (Ref. 5).

Eqs. (13) are a system of M linear equations for M unknowns, which can be solved by any standard method. The Gaussian elimination method was used for every example shown here.

With the quantities γ_m determined, the convective velocities for vortex Γ_k are known and are given by

$$\frac{dx_k}{dt} = u_k, \quad \frac{dy_k}{dt} = v_k.$$

For a system of N vortices, there are $2N$ such equations, whose solutions give the vortex trajectories. A second-order method is used for time evolution from t to $t + \Delta t$.

$$\begin{aligned}
x_k(t + \Delta t) &= x_k(t) + \frac{1}{2}[3u_k(t) - u_k(t - \Delta t)]\Delta t \\
y_k(t + \Delta t) &= y_k(t) + \frac{1}{2}[3v_k(t) - v_k(t - \Delta t)]\Delta t
\end{aligned} \tag{14}$$

At each time step, u_k and v_k must be updated by solving Eqs. (12)-(14) anew. The time step Δt is generally determined by comparing two solutions, one obtained with Δt and the other with $\Delta t/2$. If the agreement is reasonably good, the time step Δt is chosen, otherwise the process continues. It turned out that $\Delta t = 0.0125$ was adequate for every case in this study and used for most of the computations here.

Lewis has cautioned that accuracy may deteriorate, if a vortex is located very near the surface. Although this is not the case here, it is still useful to assess the accuracy. The case to be tested is a 10% thick ellipse in a uniform stream parallel to the longitudinal axis with a stationary vortex situated near the surface. Following the above procedures with a fixed vortex, a numerical solution was obtained. With the aid of the Joukowski transformation, an exact solution is also available. Shown in Fig. 3 is the comparison of surface velocity distribution between the exact and numerical solutions. The agreement is seen to be good except near the trailing edge. The accurate numerical result is mostly due to the dense distribution of surface elements (108 elements) and the accurate determination of slopes and curvatures. The latter is possible, because the geometry is known analytically.

3.1 Inner Solution and its Fourier Transform

Unlike an oscillating cylinder, which is always unsteady, the potential flow solution for body-vortex interaction involves a steady part. This part can be neglected, because a steady motion generates no sound. Therefore, only the unsteady part of the pressure will be considered. This is accomplished by means of the linearized Bernoulli equation

$$p'_i = p - p_0 = -\frac{D\phi'}{Dt} \tag{15}$$

where ϕ' refers to the unsteady part of the velocity potential and D/Dt is the time rate of change in a coordinate system moving with the undisturbed fluid velocity.

For lifting bodies with temporal loading, vortices will be shed continuously. There is a large number of mutually interacting vortices in the flow field, which are all similar. It is, therefore, possible to use one term to represent the entire group and Eq. (11) becomes

$$W = \Phi + i\Psi = \sum_{m=1}^M \frac{i\gamma_m ds_m}{2\pi} \log(z - z_m) + \frac{i\Gamma_1}{2\pi} \log[z - (t + z_{ct} + z_1)] + z \tag{16}$$

where the symbol z_{ct} denotes the initial location of a vortex, which is either far upstream of the blade or immediately behind the trailing edge for a nascent vortex just being shed. This is invariant with time. The term $t + z_{ct}$ refers to the position of a vortex at time t

convected by the freestream velocity U_0 ($U_0=1$) in the absence of the body and is “steady”. The term z_1 is the perturbed position of the vortex at time t relative to the unperturbed position, $t + z_{ct}$. Thus, only the terms γ_m and z_1 in this equation are time-dependent.

After excluding the steady part, Eq. (16) becomes

$$W' = \sum_{m=1}^M \frac{i\gamma_m ds_m}{2\pi} \log \left[z \left(1 - \frac{z_m}{z} \right) \right] + \frac{i\Gamma_1}{2\pi} \log \left[1 - \frac{(t + z_{ct}) + z_1}{z} \right] \quad (17)$$

Expanding this equation for $|z_m/z| \ll 1$, and $|z_1/z| \ll 1$, and defining $z = r \exp(i\theta)$, where θ is the angle of the receiver relative to the positive x-axis, and $z_m = \delta_m \times \exp(i\theta_m)$, one obtains

$$W' = \sum_{m=1}^M \frac{i\gamma_m ds_m}{2\pi} \left[\log r + i\theta - \frac{\delta_m}{r} e^{i(\theta_m - \theta)} \right] - \frac{i\Gamma_1}{2\pi} \frac{z_1}{z} + \dots \quad (18)$$

in which only the first order unsteady terms are retained. This equation, as written, is valid for non-lifting bodies only, where the terms involving $\log r$ and θ are zero, because with no circulation around bodies $\sum_{m=1}^M \gamma_m ds_m = \oint (\partial\phi / \partial s) ds = 0$.

For lifting bodies the unsteady Kutta condition is imposed, resulting in vortex shedding and the cancellation of the singular terms involving $\log r$ and θ in Eq. (18). In an inviscid fluid the circulation must be conserved. Thus, an incident vortex introduced in the upstream is accompanied by a vortex of opposite sense somewhere at infinity. The same argument holds true for the bound circulation for an airfoil at an angle of attack. In other words, Kelvin’s circulation theorem must be true for a large closed curve surrounding the whole system in the entire history of the motion. It follows that the Kutta condition based on the conservation of total circulation for a single blade becomes

$$\Gamma_b + \Gamma_1 + k_2 + k_3 + \dots = \Gamma_b^{(0)} + \Gamma_1 \quad (19)$$

In this equation, $\Gamma_b^{(0)}$ is the bound circulation of the blade under an angle of attack without the incident vortex and is a constant. For a symmetric body without the angle of attack, $\Gamma_b^{(0)}$ is zero. Γ_b is the bound circulation at a later time in the presence of vortices irrespective of the angle of attack, since induced velocities can create a local angle of attack. Depending on positions of the incident vortex and the vortices in the wake, the value of Γ_b changes with time. For a single blade one vortex is shed after each computational step and is placed at a distance of $\Delta t/2$ directly behind the trailing edge. Thus, the symbols k_2, k_3, \dots refer to vortices shed sequentially in time. Note that the quantity Γ_1 , the strength of the incident vortex, appears on both sides of the equation.

Although there is not a definitive form for the unsteady Kutta condition (Ref. 16), imposing it is still essential, so that the fluid leaves the trailing edge smoothly.

Obermeier (Ref. 17) used a similar form in solving the problem of rotor-vortex interaction. The present form in Eq. (19) resembles, however, that for an oscillating airfoil given in Ref. 19. This equation in conjunction with Wilkinson's method 2 in Ref. 5 constitutes the constraint that the static pressures at two trailing elements at the upper and lower surfaces be equal.

As mentioned previously, there is a singularity in Eq. (18) for a lifting body. This singularity can be removed by means of Eq. (19). To this end, Eq. (18) is rewritten as follows with the shed vortices included.

$$W' = \sum_{m=1}^M \frac{i\gamma_m ds_m}{2\pi} \log \left[z \left(1 - \frac{z_m}{z} \right) \right] + \frac{i\Gamma_1}{2\pi} \log \left[1 - \frac{z_1}{z} \right] + \frac{ik_2}{2\pi} \log \left[z \left(1 - \frac{z_2}{z} \right) \right] + \frac{ik_3}{2\pi} \log \left[z \left(1 - \frac{z_3}{z} \right) \right] + \dots \quad (20)$$

After the Kutta condition is applied and the expansion performed, this equation reduces to

$$W' = - \sum_{m=1}^M \frac{i\gamma_m ds_m}{2\pi} \frac{\delta_m}{r} \exp i(\theta_m - \theta) - \frac{i\Gamma_1 z_1}{2\pi z} - \frac{ik_2 z_2}{2\pi z} - \frac{ik_3 z_3}{2\pi z} - \dots$$

By means of the linearized Bernoulli equation, the unsteady pressure due to the body-vortex interaction in the inner region becomes

$$p'_i = \sum_{m=1}^M \frac{\partial \gamma_m}{\partial \tau} \frac{ds_m}{2\pi} \frac{\delta_m}{r} \sin(\theta - \theta_m) + \frac{\Gamma_1}{2\pi r} \left(\frac{Dx_1}{D\tau} \sin \theta - \frac{Dy_1}{D\tau} \cos \theta \right) + \frac{k_2}{2\pi r} \left(\frac{Dx_2}{D\tau} \sin \theta - \frac{Dy_2}{D\tau} \cos \theta \right) + \dots \quad (21)$$

where r and θ as before denote the radial distance and angle from the origin to the observer. $\partial \gamma_m / \partial \tau$ is the time rate of change of surface vorticity per unit length at a fixed point, while $Dx_1 / D\tau$, $Dx_2 / D\tau$, ... are the total derivatives, the differences of vortex positions observed in a coordinate system moving at the freestream speed. Since the observer is stationary but vortices are in motion, r and θ will change with time, except those measured from the surface vorticity elements to the observer. However, owing to the fact that interactions become important only when vortices are near the blade, it is therefore assumed that these variable r 's and θ 's can be approximated by the fixed r and θ from the origin to the observer. The error incurred in this approximation is small, since the present concern is with the far-field noise.

It is assumed that one vortex is shed from each trailing edge after each time step. Thus, there are two trails of wakes for a two-blade system. However, there is only one equation for the system, i.e., Kelvin's theorem. Therefore, one additional equation is needed, but it is not obvious at present how to obtain this equation. Under this circumstance, an assumption is made that Eq. (19) can be applied to each blade

independently. At first glance, it appears that this procedure decouples two blades. Fortunately, the coupling still exists, except that it is now through the application of the Kutta condition. Using Wilkinson's method 2 to unload two trailing edges, one has to solve four equations from which two simultaneous equations result. The unknowns in these two equations are Γ_b 's in Eq. (19), which are coupled. A similar assumption can be made for three or more blades. In addition, a physical interpretation also may lend support to this assumption. When blades are far apart, it is reasonable to assume that vortex shedding of one blade is independent or nearly independent from other blades. Thus, Eq. (19) may be applied individually. As they move closer, this relationship is assumed to still maintain.

Applying the Fourier transformation to Eq. (21) gives the transformed p_i'

$$\begin{aligned} \hat{p}_i' = & \frac{M_0}{2\pi} \sum_{m=1}^M \frac{ds_m \delta_m}{R} \sin(\theta - \theta_m) \int_{-\infty}^{\infty} \frac{\partial \gamma_m}{\partial \tau} e^{-i\omega\tau} d\tau \\ & + \frac{\Gamma_1 M_0}{2\pi} \left[\frac{\sin \theta}{R} \int_{-\infty}^{\infty} \frac{Dx_1}{D\tau} e^{-i\omega\tau} d\tau - \frac{\cos \theta}{R} \int_{-\infty}^{\infty} \frac{Dy_1}{D\tau} e^{-i\omega\tau} d\tau \right] \\ & + \frac{k_2 M_0}{2\pi} \left[\frac{\sin \theta}{R} \int_{-\infty}^{\infty} \frac{Dx_2}{D\tau} e^{-i\omega\tau} d\tau - \frac{\cos \theta}{R} \int_{-\infty}^{\infty} \frac{Dy_2}{D\tau} e^{-i\omega\tau} d\tau \right] + \dots \end{aligned} \quad (22)$$

where M_0 is the freestream Mach number and $R = M_0 r$.

4. OUTER SOLUTION, ASYMPTOTIC MATCHING, AND INVERSE TRANSFORM

The governing equation in the outer region is Eq. (4). The solution of this equation is suggested by the inner solution and is assumed to be

$$\begin{aligned} p_o' = & \sum_{m=1}^M p_m(R, t) \sin(\theta_m - \theta) + [p_{1s}(R, t) + p_{2s}(R, t) + \dots] \sin \theta \\ & + [p_{1c}(R, t) + p_{2c}(R, t) + \dots] \cos \theta \end{aligned} \quad (23)$$

where p_m , p_{1s} , p_{1c} , p_{2s} , p_{2c} , ... are functions to be determined. Substituting Eq. (23) into Eq.(4) and performing the Fourier transform result in a set of ordinary differential equations, all of which are of the form of Eq. (6), whose solutions for outgoing waves are the Hankel functions of the second kind. Thus, Eq. (23) becomes

$$\begin{aligned} \hat{p}_o' = & \sum_{m=1}^M A_m H_1^{(2)}(\omega R) \sin(\theta - \theta_m) \\ & + (A_{1s} + A_{2s} + \dots) H_1^{(2)}(\omega R) \sin \theta + (A_{1c} + A_{2c} + \dots) H_1^{(2)}(\omega R) \cos \theta \end{aligned} \quad (24)$$

where $A_m, A_{1s}, A_{1c} \dots$ are the unknown coefficients to be determined by matching. For example, A_m 's are the coefficients for the surface pressure fluctuations, A_{1s} and A_{1c} are for the moving vortex, and the remaining ones are for the shed vortices.

The steps for matching are the same as for the oscillating cylinder. When this is done, Eq.(24) becomes

$$\begin{aligned} \hat{p}'_o = & -\frac{iM_0\omega}{4} \sum_{m=1}^M ds_m \delta_m \sin(\theta - \theta_m) H_1^{(2)}(\omega R) \int_{-\infty}^{\infty} \frac{\partial \gamma_m}{\partial \tau} e^{-i\omega\tau} d\tau \\ & -\frac{i\Gamma_1 M_0 \omega}{4} H_1^{(2)}(\omega R) \left[\sin\theta \int_{-\infty}^{\infty} \frac{Dx_1}{D\tau} e^{-i\omega\tau} d\tau - \cos\theta \int_{-\infty}^{\infty} \frac{Dy_1}{D\tau} e^{-i\omega\tau} d\tau \right] \\ & -\frac{ik_2 M_0 \omega}{4} H_1^{(2)}(\omega R) \left[\sin\theta \int_{-\infty}^{\infty} \frac{Dx_2}{D\tau} e^{-i\omega\tau} d\tau - \cos\theta \int_{-\infty}^{\infty} \frac{Dy_2}{D\tau} e^{-i\omega\tau} d\tau \right] - \dots \end{aligned}$$

where k_2, k_3, \dots refer to the strengths of shed vortices and are zero for non-lifting bodies. This equation, after the inverse Fourier transform, yields the acoustic pressure in the far field

$$\begin{aligned} p'_o = & -\frac{iM_0}{8\pi} \sum_{m=1}^M ds_m \delta_m \sin(\theta - \theta_m) \int_{-\infty}^{\infty} \omega H_1^{(2)}(\omega R) e^{i\omega t} d\omega \int_{-\infty}^{\infty} \frac{\partial \gamma_m}{\partial \xi} e^{-i\omega\xi} d\xi \\ & -\frac{i\Gamma_1 M_0}{8\pi} \sin\theta \int_{-\infty}^{\infty} \omega H_1^{(2)}(\omega R) e^{i\omega t} d\omega \int_{-\infty}^{\infty} \frac{Dx_1}{D\xi} e^{-i\omega\xi} d\xi \\ & +\frac{i\Gamma_1 M_0}{8\pi} \cos\theta \int_{-\infty}^{\infty} \omega H_1^{(2)}(\omega R) e^{i\omega t} d\omega \int_{-\infty}^{\infty} \frac{Dy_1}{D\xi} e^{-i\omega\xi} d\xi \\ & -\frac{ik_2 M_0}{8\pi} \sin\theta \int_{-\infty}^{\infty} \omega H_1^{(2)}(\omega R) e^{i\omega t} d\omega \int_{-\infty}^{\infty} \frac{Dx_2}{D\xi} e^{-i\omega\xi} d\xi \\ & +\frac{ik_2 M_0}{8\pi} \cos\theta \int_{-\infty}^{\infty} \omega H_1^{(2)}(\omega R) e^{i\omega t} d\omega \int_{-\infty}^{\infty} \frac{Dy_2}{D\xi} e^{-i\omega\xi} d\xi + \dots \quad (25) \end{aligned}$$

It represents the time history of the far-field sound pressure from the far upstream to the end of computation. However, its value becomes appreciable only in the short interval when the vortex is near the body. Outside of this range the medium is essentially silent. This property of fast decay can also be seen in the linear theory of Howe (Ref. 19).

4.1 Discrete Fourier Transform

At first glance, it appears to be uncertain whether the function in the inverse transform is absolutely integrable, since $\omega H_1^{(2)}(\omega R)$ in Eq. (25) approaches $\omega^{1/2}$ as $\omega \rightarrow \infty$. However, due to the fast decay vortex interaction terms, such as

$\int_{-\infty}^{\infty} \partial \gamma_m / \partial \xi e^{-i\omega \xi} d\xi$, approach $1/\omega^2$ at infinity. The function as a whole is absolutely integrable. The remaining work is to evaluate these integrals numerically by means of, say, the discrete Fourier transform.

In order to establish some confidence that the execution of the discrete Fourier transform as given in Ref. 13 is done correctly, Crighton's solution in Ref. 7 is computed numerically. The comparison is shown in Fig. 4 and the agreement is seen to be good. In this figure, the scaling factor $M^{1/2} \sin(\theta/2)/r_{cr}^{1/2}$ for the acoustic potential in his Eq. (3.6) was not included and the value for r_{cr} was chosen to be 15.0. The maximum value of the potential is at $t = r_{cr}$ and the decay is very slow. This is in striking contrast with the vortex interaction of finite bodies, in which the sound pressure decays rapidly once the vortex passes the body.

5. CASCADE-VORTEX INTERACTION

5.1 Inner Solution

A cascade is an infinite array of similar blades and cannot in general be regarded as a compact body. However, if one agrees to the viewpoint that the flow property of a single blade in a computational domain with appropriate periodic boundary conditions can represent that of a cascade, a cascade may then be considered to be compact. Based on this assumption, an attempt may then be made to study sound generation of a cascade-vortex interaction.

The complex potential for a series of vortices of equal strength placed uniformly at points $z_0 \pm ikb$ along the y-axis is (Ref. 5 or 20)

$$W = \frac{i\Gamma}{2\pi} \log \sinh \left[\frac{\pi}{b} (z - z_0) \right],$$

Upon substitution of $\gamma_m ds_m$ for Γ as was done for a single blade, the complex potential in the inner region of a cascade in a uniform stream together with a series of moving vortices of strength Γ_s at points $z_s \pm ikb$ becomes

$$W_i = \sum_{m=1}^M \frac{i\gamma_m ds_m}{2\pi} \log \sinh \left[\frac{\pi}{b} (z - z_0) \right] + \frac{i\Gamma_s}{2\pi} \log \sinh \left[\frac{\pi}{b} (z - z_s) \right] + z \quad (26)$$

where the subscript i denotes the complex potential in the inner region. Since there is only one vortex in each blade pitch, b refers also to the pitch of vortices.

This equation bears a close resemblance to Eq. (11). Therefore, it is reasonable to expect that there is a counterpart of Eq. (13) for a cascade, whose influence coefficients are

$$K_c(s_n, s_m) = \frac{-\sinh \frac{2\pi}{b} (x_n - x_m) \sin \theta_n + \sin \frac{2\pi}{b} (y_n - y_m) \cos \theta_n}{\cosh \frac{2\pi}{b} (x_n - x_m) - \cos \frac{2\pi}{b} (y_n - y_m)}$$

$$K_s(s_n, s_s) = \frac{-\sinh \frac{2\pi}{b} (x_n - x_s) \sin \theta_n + \sin \frac{2\pi}{b} (y_n - y_s) \cos \theta_n}{\cosh \frac{2\pi}{b} (x_n - x_s) - \cos \frac{2\pi}{b} (y_n - y_s)},$$

where most symbols have similar meanings as in Eq. (13). In particular, K_c corresponds K_b in Eq. (13) and K_s to K_v . For more details, see Ref. 5 or 20. The quantities γ_m and the vortex trajectories are determined in a similar manner as for a single blade.

The cascade blades are assumed to be lifting bodies and the Kutta condition has to be imposed. This will result in arrays of shed vortices in wakes behind trailing edges. These terms must be added to Eq. (26) to form a complete system. When this is done, the velocity potential becomes

$$\phi_i = -\sum_{m=1}^M \frac{\gamma_m ds_m}{2\pi} \tan^{-1} \left[\frac{\tan \frac{\pi}{b} (y - y_m)}{\tanh \frac{\pi}{b} (x - x_m)} \right] - \frac{\Gamma_s}{2\pi} \tan^{-1} \left[\frac{\tan \frac{\pi}{b} (y - y_s)}{\tanh \frac{\pi}{b} (x - x_s)} \right]$$

$$- \frac{k_2}{2\pi} \tan^{-1} \left[\frac{\tan \frac{\pi}{b} (y - y_2)}{\tanh \frac{\pi}{b} (x - x_2)} \right] - \dots \quad (27)$$

where k_2, k_3, \dots refer to arrays of vortices shed at each computational step with the same pitch as for the blades. In the limit of large $|z|$ or $|x_i/x| \ll 1$, where the subscript i denotes $m, s, 2$ or $3 \dots$ in the above expression, Eq. (27) reduces to

$$\phi_i = -\sum_{m=1}^M \frac{\gamma_m ds_m}{2b} (y - y_m) - \frac{\Gamma_s}{2b} (y - y_s) - \frac{k_2}{2b} (y - y_2) - \frac{k_3}{2b} (y - y_3) - \dots \quad (28)$$

This equation is singular, since terms become arbitrarily large as $y \rightarrow \pm\infty$. To remove this singularity, recourse is made to the Kutta condition, which assumes a similar form as for a single blade

$$\Gamma_b + \Gamma_s + k_2 + k_3 + \dots = \Gamma_b^{(0)} + \Gamma_s$$

The notations in this equation are essentially the same as for a single blade, except that their meanings are slightly different. After the singularities are removed, Eq. (28) together with the linearized Bernoulli equation Eq. (5) gives

$$p'_i = - \sum_{m=1}^M \frac{ds_m}{2b} y_m \frac{\partial \gamma_m}{\partial t} - \frac{\Gamma_s}{2b} \frac{Dy_s}{Dt} - \frac{k_2}{2b} \frac{Dy_2}{Dt} - \frac{k_3}{2b} \frac{Dy_3}{Dt} - \dots$$

where p'_i denotes the perturbed pressure in the inner region. The Fourier transform of this equation is

$$\hat{p}'_i = - \sum_{m=1}^M \frac{ds_m}{2b} y_m \int_{-\infty}^{\infty} \frac{\partial \gamma_m}{\partial t} e^{-i\omega t} dt - \frac{\Gamma_s}{2b} \int_{-\infty}^{\infty} \frac{Dy_s}{Dt} e^{-i\omega t} dt - \frac{k_2}{2b} \int_{-\infty}^{\infty} \frac{Dy_2}{Dt} e^{-i\omega t} dt - \dots \quad (29)$$

5.2 Outer Solution and Matching

The acoustic equation in the outer region is given as

$$\frac{\partial^2 p'_0}{\partial X^2} + \frac{\partial^2 p'_0}{\partial Y^2} - \frac{\partial^2 p'_0}{\partial t^2} = 0,$$

where X and Y are the rescaled coordinates, $X = M_0 x$ and $Y = M_0 y$. In view of the inner solution, which involves t and x only, the Y term in the above equation may be dropped resulting in a one-dimensional wave equation

$$\frac{\partial^2 p'_0}{\partial X^2} - \frac{\partial^2 p'_0}{\partial t^2} = 0. \quad (30)$$

This simplification is in agreement with our intuitive notion that the sound wave in the far field from an infinite array of blades should be independent of Y .

The Fourier transform of Eq. (30) gives

$$\frac{d^2 \hat{p}'_0}{dX^2} + \omega^2 \hat{p}'_0 = 0,$$

whose solution is $\hat{p}'_0 = A e^{\pm i\omega X}$. In the limit of $x \rightarrow 0$, it becomes $\hat{p}'_0 \cong A$. The quantity A may then be evaluated by matching with Eq. (29). After this is done and the inverse Fourier transform is applied, the sound pressure in the far field becomes

$$p'_0 = - \sum_{m=1}^M \frac{ds_m}{4\pi b} y_m \int_{-\infty}^{\infty} \int_{-\infty}^{\infty} \frac{\partial \gamma_m}{\partial \xi} e^{-i\omega \xi} d\xi e^{i\omega(t \pm X)} d\omega$$

$$- \frac{\Gamma_s}{4\pi b} \int_{-\infty}^{\infty} \int_{-\infty}^{\infty} \frac{Dy_s}{D\xi} e^{-i\omega \xi} d\xi e^{i\omega(t \pm X)} d\omega - \frac{k_2}{4\pi b} \int_{-\infty}^{\infty} \int_{-\infty}^{\infty} \frac{Dy_2}{D\xi} e^{-i\omega \xi} d\xi e^{i\omega(t \pm X)} d\omega \dots$$

Under the assumption that changing the order of integration is permissible, this equation can be greatly simplified. Using the second term as an example, one obtains

$$\begin{aligned} -\frac{\Gamma_s}{4\pi b} \int_{-\infty}^{\infty} \frac{Dy_s}{D\xi} d\xi \int_{-\infty}^{\infty} e^{i\omega(t-\xi-x)} d\omega &= -\frac{\Gamma_s}{2b} \int_{-\infty}^{\infty} \frac{Dy_s}{D\xi} \delta(t-\xi-M_0x) d\xi \\ &= -\frac{\Gamma_s}{2b} \left(\frac{Dy_s}{D\xi} \right)_{t-M_0x} \end{aligned}$$

The subscript $t-M_0x$ denotes the retarded time. As seen, only the wave traveling in the positive x -direction is retained. With this development, the above equation reduces to

$$p'_0 = -\sum_{m=1}^M \frac{ds_m}{2b} y_m \left(\frac{\partial \gamma_m}{\partial t} \right)_{t-M_0x} - \frac{\Gamma_s}{2b} \left(\frac{Dy_s}{Dt} \right)_{t-M_0x} - \frac{k_2}{2b} \left(\frac{Dy_2}{Dt} \right)_{t-M_0x} - \dots \quad (31)$$

This is the final form of the first approximation for sound pressure of the cascade in the far field. It propagates outward without distortion and with no diminution of amplitude except that the arriving time is somewhat delayed. These are the characteristics of a one-dimensional wave. The intensity is inversely proportional to the pitch.

6. RESULTS AND DISCUSSION

Before presenting any results, it is worth making a comparison between a computation and an experiment. Unfortunately, there is a scarcity of experimental data for this problem and it appears that only an order-of-magnitude comparison is possible. Booth's data (Ref. 21) will be used here for comparison. However, there is at least one major difference between the test and computation. Vortices in his experiment either burst or split into fragments before reaching the blade. This condition cannot be simulated in the present computation and is likely to lead to a disagreement. In addition, the measured pressure, on which the experimental sound production is based, included only 25% of the surface pressure fluctuation and neglected other sound producing mechanisms. The acoustic field in Ref. 21 was evaluated in front of the blade, where the magnitude is very small. This may be another source of the difference. In spite of these discrepancies, a comparison may still be useful.

There were four different vortex trajectories recorded in Ref. 21 for the zero angle-of-attack case. The case of $y/c = -0.219$ was chosen for comparison, because the blade-to-vortex miss distance was the largest. This value is equivalent to $y_v = -0.156$ in the computation, a distance of 0.156 chord lengths below the centerline. The measured vortex strength was given as $0.49 \text{ m}^2/\text{sec.}$, which is equivalent to $\Gamma = 0.524$, a vortex of high intensity in an extremely low free stream. For the convenience of comparison, the calculated dimensionless quantities have been converted to the

dimensional quantities in pascals and seconds as used in Ref. 21. The area between two dashed curves represents approximately the range of test data in Booth's Fig. 6b.

The predicted acoustic pressure shown in Fig. 5 consists of three parts: the unsteady surface pressure, the moving vortex and the wake. Although the sound production by the wake is usually negligible, the application of the Kutta condition is still important, since without it the temporal variation of the surface pressure will not be correct. No plot of the wake is given here, but it will be shown later in another example. Its influence can, however, be seen in the insert in Fig. 5, where the vortex trajectory is bent slightly downward. This bending was also mentioned in Ref. 17. For various reasons mentioned above, the comparison in Fig. 5 can only be considered as an order-of-magnitude comparison.

6.1 Single Blade

After this digression, we now return to the main concern with vortex interaction. Shown in Figs. 6 and 7 are four examples of one incident vortex interacting with a symmetric blade (NACA 0012). These interactions, though simple, play an important role as interferences and more complex cases are to be examined. For this reason, some explanations are in order.

The observer in both figures is directly above the blade at a distance of 50 chord lengths from the leading edge, which is the origin of the coordinate system, and at 90° from the positive x-axis ($r = 50$ and $\theta = \pi/2$). The freestream Mach number M_0 is 0.2. (Except as stated, $r = 50$, $\theta = \pi/2$ and $M_0 = 0.2$ for every computation henceforth.) The initial position of the vortex is 5 chord lengths upstream of the leading edge in the x-direction and ± 0.1 chord lengths in the y-direction ($x_v = -0.5$ and $y_v = \pm 0.1$). The sense of the vortex is either positive or negative (positive when clockwise in accordance with Lewis' convention). The vortex passes above the blade in Figs. 6 and below the blade in Figs. 7.

The sound pressure in Fig. 6a is caused by a counter-clockwise rotating vortex. If its sense is reversed with all other parameters remaining unchanged, the sign of the sound pressure also will be reversed and the magnitude will be slightly higher. In addition, the vortex trajectory and the vortex-to-blade miss distance are somewhat different (Fig. 6b). These variations are due to the different manners that an incident vortex interacts with the blade. It is said that a vortex produces sound mainly when it cuts across base flow streamlines near an edge (see, for example, Howe or Ref. 11).

In computations with lifting bodies, wakes always occur due to the local angles of attack brought about by the induced velocities even though blades are parallel to the freestream. Thus, in the examples of Figs 6 and 7 a part of the solution is the trail of shed vortices (wake), but this is not shown in the above figures because of the limited space. An example of the wake pattern, however, will be given in Fig. 14b.

Figs. 7 depicts two examples for the vortex passing below the blade. The acoustic pressure in Fig. 7a is equal to that in Fig. 6b, except the sign. From the viewpoint of noise attenuation, this property of sign reversal is significant and will be exploited later. Since the body is symmetric, this case is equivalent to the case of a clockwise rotating vortex passing above the blade with the observer below the body. By the same token, the acoustic pressure in Fig. 7b is a counterpart of Fig. 6a.

To present a more complete picture, the directivity pattern for Fig. 6a is shown in Fig. 8a and is seen to be akin to that of a dipole. The patterns for others in Figs. 6-7 are similar and will not be given. The directivities here are the standard polar diagrams with the rms pressures as the radial distances. The sample time for the root mean square is somewhat arbitrary and was taken to be the range where the sound pressure is visually discernible. The origin of the coordinates is at the leading edge of the blade or at the leading edge of the upper blade, if two blades are present. The maximums in Fig. 8a occur at $\theta = \pi/2$ and $3\pi/2$. The former corresponds to the observer's position in Figs. 6a.

Knowing the occurrence of sound pressure of opposite signs, one can take advantage of this property to reduce noise. In an ideal situation such as that in Fig. 9a, the cancellation is complete and sound is absent. Normally even if there is no sound produced by the surface, the wake, if it exists, can still generate sound of very low intensity. In this case of total destructive interference, the Kutta condition is automatically satisfied and there is no wake. For this reason, the directivity is also zero.

For the complete destruction to occur, the blade has to be symmetric, and vortices are of equal magnitude, opposite sense and at an equal distance from the blade. They also must pass the blade concurrently. The last condition of concurrent arrival is a very stringent requirement. In other words, the initial positions of these two vortices must be equal horizontally. If instead of two isolated vortices, there are two streams of closely packed vortices, some of them will probably arrive almost concurrently.

Two vortex paths in Fig. 9a are symmetric with respect to the blade. This is desirable but is not essential. For instance, the noise attenuation in Fig. 9b is still substantial, even though the lower vortex path in Fig. 9b is 1.5 times farther from the chord than the upper path. In comparison with a single vortex in Fig. 6a, the overall noise intensity is lower and the corresponding directivity in Fig. 8b is also considerably smaller.

Thus far the strengths of both vortices are equal. This need not be the case as shown in Fig. 10a, in which the vortex paths are not symmetric, the strengths are not equal and yet the noise is lower.

The above are three examples with two incident vortices, one on each side. In the following, examples are given with both vortices on the same side of the blade. This is to demonstrate that the primary reason of noise attenuation is the presence of a pair of vortices of opposite sense as in Fig. 10b. Notice that the induced velocities by vortices on themselves are in the opposite direction of the free stream. Thus, the arrival time at the blade is delayed, which is reflected by the longer time for the peak pressure to appear. The converse also is true. In this case, the signals will be somewhat clustered.

Two more examples will be presented for a single blade. One is the case that the blade is at an angle of attack of 5° . The attenuation in Fig. 11a is considerable. This is mainly due to the small separation distance between two vortices and not to the angle of attack. If this distance decreases further, destructive interference also will be larger. The second case is shown in Fig. 11b, where a pair of vortices of same sense is convected by the free stream while rotating about their centroid. Based on the previous assumption that attenuation is the result of two vortices of opposite sense, one may anticipate a twofold increase in noise in Fig. 11b as compared with Fig. 6a. This

is, however, not the case. The reason may be that the blade-vortex interaction for a rotating pair is sufficiently complex that cannot be explained by the simple addition. The evidence here and elsewhere indicates that a pair of rotating vortices acts somewhat like a single vortex as far as sound production is concerned. Note that a pair of spinning vortices without any blade will also produce sound (Ref. 6). However, its intensity is very low and cannot be easily discerned in this figure.

6.2 Two or More Blades

Since the present method is not limited to a single body, attention is now directed to vortex interactions involving two or more blades with two or more incident vortices. One example in this group is a pair of stacked blades somewhat like a two-dimensional inlet with a single vortex moving through the passage as in Fig. 12a. The separation distance between two blades is sufficiently large, so that the blade-to-blade influence is relatively small. The resulting sound pressure is, therefore, similar to that of Fig. 7a for a single blade. Note that two blades parallel to a uniform stream in the absence of incident vortices can still induce circulation on each other, but the total strength of circulations is zero in accordance with Kelvin's theorem.

Although the directivity pattern for this case, if plotted, is similar to Fig. 8a, a radical change can take place, if another vortex is introduced. For instance, the sound pressure in Fig. 12b received at $\theta = \pi/2$ is nearly zero. At first glance, one may think that this is a case of complete destructive interference. This is, however, not the case after seeing the directivity diagram in Fig. 8c. The overall intensity is actually increased but the directivity pattern has rotated 90° with the minimums in the vertical direction where the signal is received. Attenuation is still possible by simply shifting the lower vortex upward as illustrated in Fig. 13a. Although the magnitude of sound pressure in this figure is not too much smaller than others, the overall intensity is lower as can be seen by comparing the directivity of Fig. 8c with that of Fig. 8d. The latter is the directivity pattern for Fig. 13a. Moreover, the configuration in Fig. 8d is rotated and the mid-section is bulged out. The direction of maximum sound intensity is, therefore, different. The lower vortex in this case interacts with both blades, since it passes through almost the middle of the passageway. This likely is the underlying mechanism of attenuation. In order to see this effect, the sound pressures from both blades are plotted separately in Fig. 13b. In this figure, the extent of attenuation, though not large, can clearly be seen. Note also that for the purpose of attenuation the precise position of the lower vortex is not critical, as long as it falls within a certain range.

A further reduction of sound generation is possible, if two blades form a divergent-like "channel" as in Fig. 14a. The geometry of the blades is the same as before, except the outward rotations of 5° . The upstream positions for two incident vortices in this case are also the same as in Fig. 13a. Since two blades rotate outward and the vortex-to-blade miss distances become larger, reduction in sound intensity is expected. The extent of reduction as shown in Fig. 15a is, however, not foreseen.

Before proceeding any further, it is time to include a snapshot of the wake formation behind the blades. As mentioned previously, the Kutta condition is imposed in computations with lifting bodies. Therefore, wakes, though not plotted, are a part of

solutions. The configuration in Fig. 14b should be a part of the insert in Fig. 14a, if more space is available. The two blades in Fig. 14b correspond to the blades in the insert of Fig. 14a. In the present formulation and for the convenience of bookkeeping, one vortex is shed from each trailing edge at every time step regardless of its strength. For instance, when the incident vortex is far from the body, the circulation around a large closed curve is essentially invariant, and yet the Kutta condition is still applied and vortices are still shed. The strengths of these vortices are nearly zero, which manifest as straight lines in Fig. 14b. Only the curved portions are created while vortices pass near the blades and contain significant vorticities.

As anticipated, a pair of like-signed vortices convected through an inlet-like passage will cause the noise level to increase as indicated in Fig. 16a and the accompanied directivity plot in Fig. 15b. Although a similar technique as in Fig. 13a can be used to reduce noise level by lifting the lower vortex trajectory upward, the underlying mechanism appears to be different. With two vortices of same sense, each will rotate about the centroid with a constant speed. The end result is to cause vortices moving away from the blades and, therefore, to lessen sound production. Thus, as long as there are two vortices in the passage, a judicious arrangement of their positions can promote destructive interference.

In Section 6.1, two examples were given to demonstrate that: (a) sound production is not affected materially by the angle of attack (Fig. 11a), and (b) a pair of rotating vortices acts more like a single vortex than two separate vortices (Fig. 11b). These properties are found to be essentially valid for two stacked blades.

In the preceding examples, the separation distance between two blades was fixed to be of one chord length. Change of this distance is expected to have an effect on sound production. However, a decrease of this distance by a moderate amount does not seem to have much effect on the noise intensity or the directivity pattern (Figs. 16b and 15c), while an increase by a similar amount proportionally elevates the intensity substantially (Figs. 17a and 15d). The reason appears to be that as the separation distance increases, sound production from the upper blade and from the lower blade becomes essentially additive with little coupling between them, and the intensity becomes higher. As the distance reduces, the coupling increases, more attenuation results and the intensity becomes lower. Note that the observer's position in Figs. 16b and 17a is at $\theta = 45^\circ$, so that the received sound pressure is not zero. If it were 90° , sound pressure will be zero as in the case of Fig. 12b.

Although the separation distance does not have a major effect on sound production, staggering (two leading edges are not aligned vertically) does. This is somewhat equivalent to the non-concurrent arrival of two vortices. Thus, the more it is staggered, the higher is the sound. The effect of staggering is shown in Fig. 17b. In view of its directivity pattern in Fig. 18a, the noise intensity has been greatly increased. Note that the receding distance of the lower blade is relatively small and equals 0.25 chord lengths. There are two methods to bring down noise in this case. One is the usual procedure of repositioning vortices to attenuate sound generation. This method will not be repeated here. The other is to reduce the size of the lower blade. The reduction in noise is only moderate and is shown in Figs. 18b and 19a.

As the observer moves farther away from the interaction, the received sound is expected to decrease. The relationship is not exactly linear as can be seen in Eqs. (10)

and (25). In order to see this effect, Fig. 19b is included in which the observer is 100 chord lengths from the origin as opposed to the usual distance of 50 chord lengths with all other parameters unchanged.

Next consideration is given to the case of three vortices interacting with 3 stacked blades (Fig. 20b). In order to see the difference between this configuration and the corresponding case of two blades, Fig. 20a is first calculated, whose directivity pattern is in Fig. 18c. Both the size and shape of this pattern are seen to be somewhat similar to those in Fig. 15b. This seems to be reasonable, since in these two cases the strengths of vortices are equal, they are all negative and the vortex-to-blade miss distances are nearly equal, although the dispositions of vortices are different. The case of 3 blades in Fig. 20b is merely an extension of Fig. 20a as is evident by comparing these two figures. The unsettled question is whether its acoustic characteristics will approach asymptotically to that of a linear cascade as the number of stacked blades increases.

6.3 Nonlifting Bodies

In all previous cases, only lifting bodies have been studied. It would be of interest to give two examples corresponding to two previous cases but with nonlifting bodies. In these cases there will not be any wake and there is no need to impose the Kutta condition. However, it was found that the calculated circulation around the body, though small, was not in general zero. This discrepancy has to be removed, because if the circulation is not zero, the singularity in Eq. (18) will prevail, which will then have an adverse effect on the sound production. In order to impose this zero circulation condition, a procedure similar to Wilkinson's method 2 for the Kutta condition was employed.

The first example is similar to Fig. 6a and is shown in Fig. 21a. It is interesting to note that there is no high peak in the sound production and the overall intensity is considerably lower than that in Fig. 6a. The sound pressure distribution is seen to be antisymmetric with respect to the mid-point. This is likely due to the symmetry of the body. The second example is a counterpart of Fig. 10b. Here the destructive interference is obvious and is more effective than that for a lifting body. In view of these two examples, it seems to indicate that if a lifting body can be replaced by a nonlifting body, the noise production by vortex interaction will be markedly lower. Although not evident, the geometry of this non-lifting body bears similarity to an NACA-0012 airfoil in the sense that it is essentially formed by two front halves of the airfoil. Its thickness is also approximately equal to 12% of the length. Thus, a large decrease in noise production by non-lifting bodies is likely due to the absence of the trailing edge.

7. CONCLUSION

The results of this study may be summarized as follows: (a) In the section of method validation, it is shown explicitly that the method of matched asymptotic expansions is a viable method for analyzing sound generation. (b) A procedure is devised to examine the interaction of multiple bodies with multiple vortices. (c) Under various

conditions, it is demonstrated that destructive interference is a possible mechanism for suppressing noise production. (d) A solution to sound generation by cascade-vortex interaction is given. (e) Based on numerical results, it appears that sound generation by vortex interaction with nonlifting bodies is much lower than that with lifting bodies.

REFERENCES

1. Dittmar, J.H., "Interaction of rotor tip flow irregularities with stator vanes as a noise source," AIAA paper 77-1342, Nov. 1977.
2. Shaw, L.M. and Bolombin, J.R., "Rotor wake characteristics relevant to rotor-stator interaction noise generation," *J. Aircraft*, **19**, 1982, 954-962.
3. George, A.R., "Helicopter noise: state-of-the-art," *J. Aircraft*, **15**, 1978, 707-715.
4. Dowling, A.P. and Ffowcs Williams, J. E., *Sound and sources of sound*, John Wiley, 1983.
5. Lewis, R.I., *Vortex element methods for fluid dynamic analysis of engineering systems*, Cambridge Univ. Press, New York, 1991.
6. Muller, E.A. and Obermeier, F., "The spinning vortices as a source of sound," AGARD CP-22, 1967, 22.1-22.8.
7. Crighton, D.G., "Radiation from vortex filament method near a half plane," *J. Fluid Mech.*, **51**, 1972, 357-362.
8. Davis, S.S., "Theory of discrete vortex noise," *AIAA J.*, **13**, 1975, 375-380.
9. Hardin, J.C., "Noise radiation form the side edges of flaps," *AIAA J.*, **18**, 1980, 549-552.
10. Consluk, A.T. and Veley, D., "The generation of noise in impinging vortex motion past a step," *Phy. Fluids*, **28**, 1985, 3004-3012.
11. Sen R., "Vortex-oscillation model of airfoil side-edge noise," *AIAA J.*, **35**, 1997, 441-449.
12. Hu, F.Q., Martin, J.E. and Hussaini, M.Y., "On computing sound radiation of temporally evolving mixing layer by vortex method and matched asymptotic expansions," AIAA paper 96-0875, 1996.
13. Brigham, E.O., *The fast Fourier transform*, Prentice-Hall, 1974.
14. Van Dyke, M., *Perturbation methods in fluid mechanics*, The Parabolic Press, 1975.
15. Abramowitz, M. and Stegun, I.A., *Handbook of mathematical functions*, Dover, 1965.
16. Crighton, D.G., "The kutta condition in unsteady flow," in *Annual Review of Fluid Mech.*, **17**, 1985, 411-445.
17. Obermeier, F., "Sound generation by rotor-vortex interaction in subsonic flow," AIAA Paper 90-3974, Oct. 1990.
18. Ham, N.D., "Aerodynamic loading on a two-dimensional airfoil during dynamic stall," *AIAA J.*, **6**, 1968, 1927-1934.
19. Howe, M.S., "The influence of vortex shedding on the generation of sound by convected turbulence," *J. Fluid Mech.*, **76**, 1976, 711-740.
20. Gostelow, J.P., *Cascade aerodynamics*, Pergamon Press, 1984.
21. Booth, E.R., "Experimental observations of two-dimensional blade-vortex interaction," *AIAA J.*, **28**, 1990, 1353-1359.

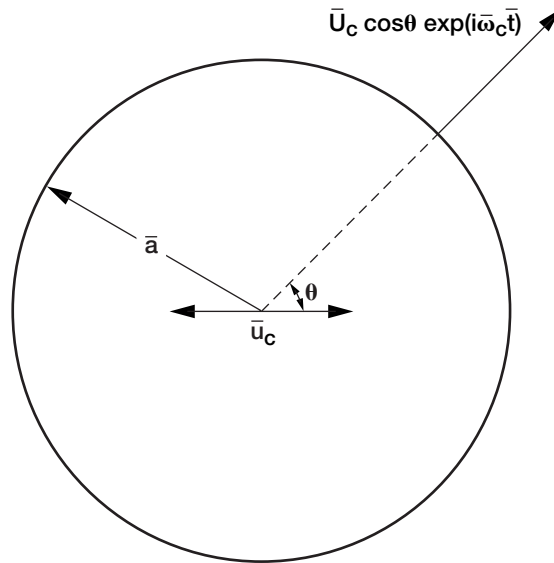


Figure 1.—Cylinder oscillating in the x-direction.
 $\bar{u}_c = \bar{U}_c \exp(i\bar{\omega}_c \bar{t})$.

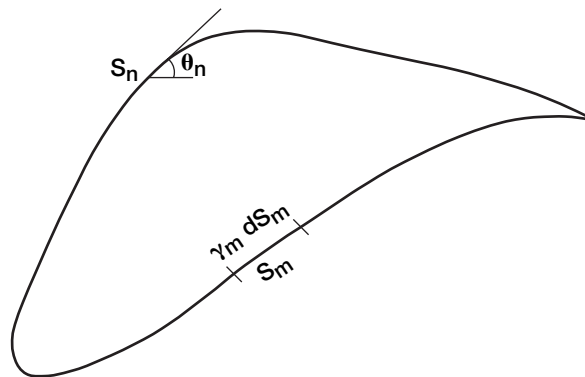


Figure 2.—Surface vorticity elements on a two-dimensional body.

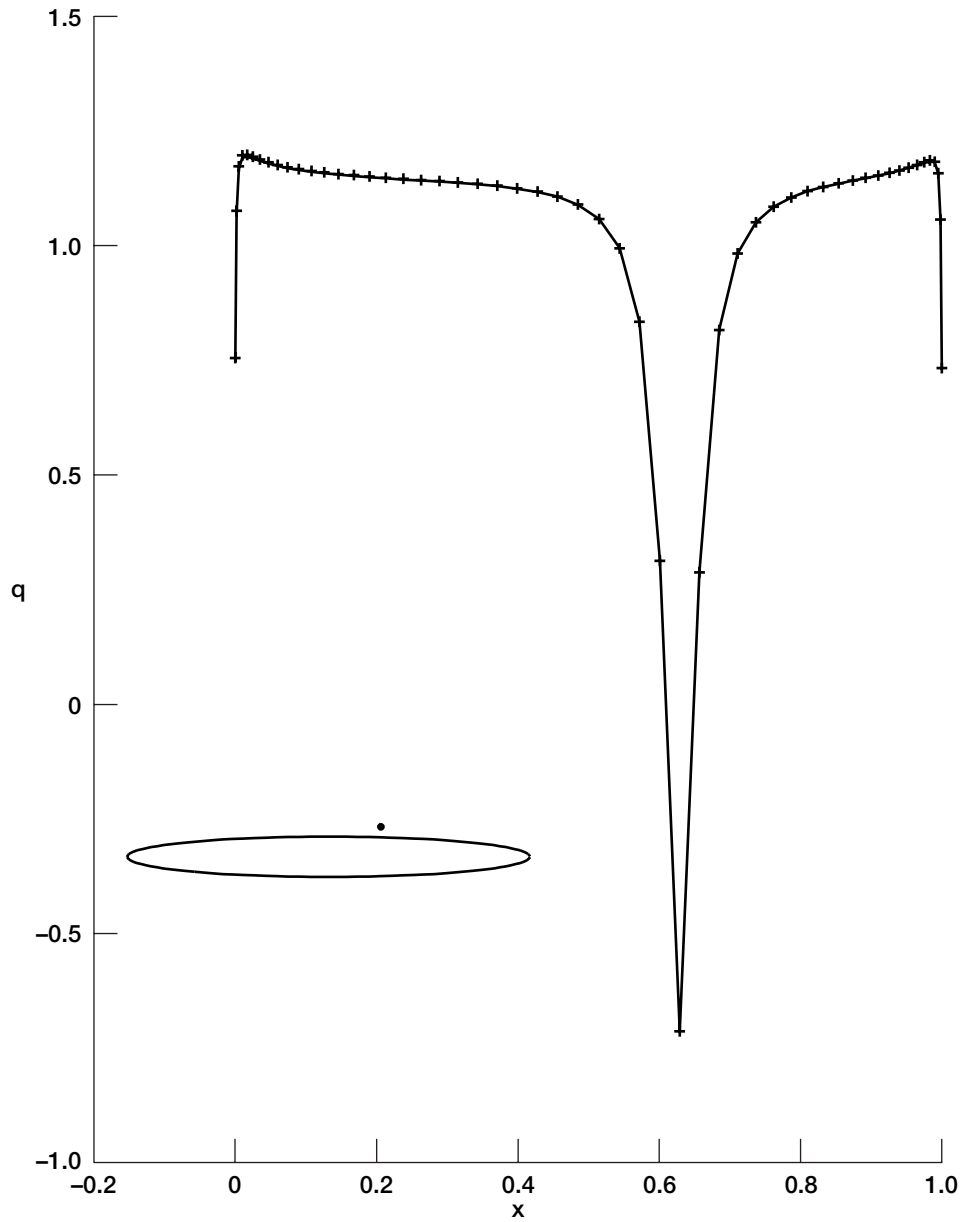


Figure 3.—Velocity distribution on upper surface of a thin ellipse in a uniform stream with an external vortex. Thickness to chord ration = 0.1; angle of attack = 0; —, exact solution; +, numerical solution; *, vortex location.

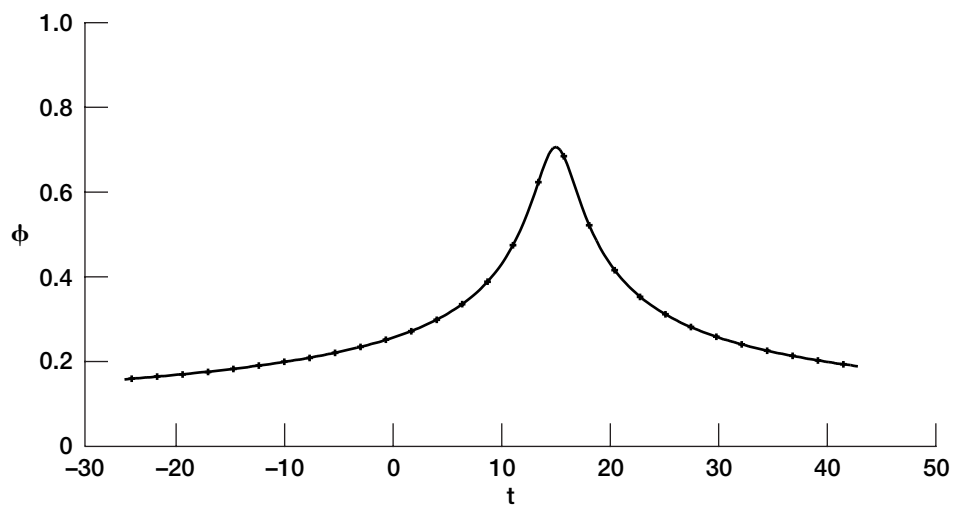


Figure 4.—Numerical evaluation of Fourier integrals compared with Crighton's analytic solution of acoustic potential. —, analytic; +, numerical.

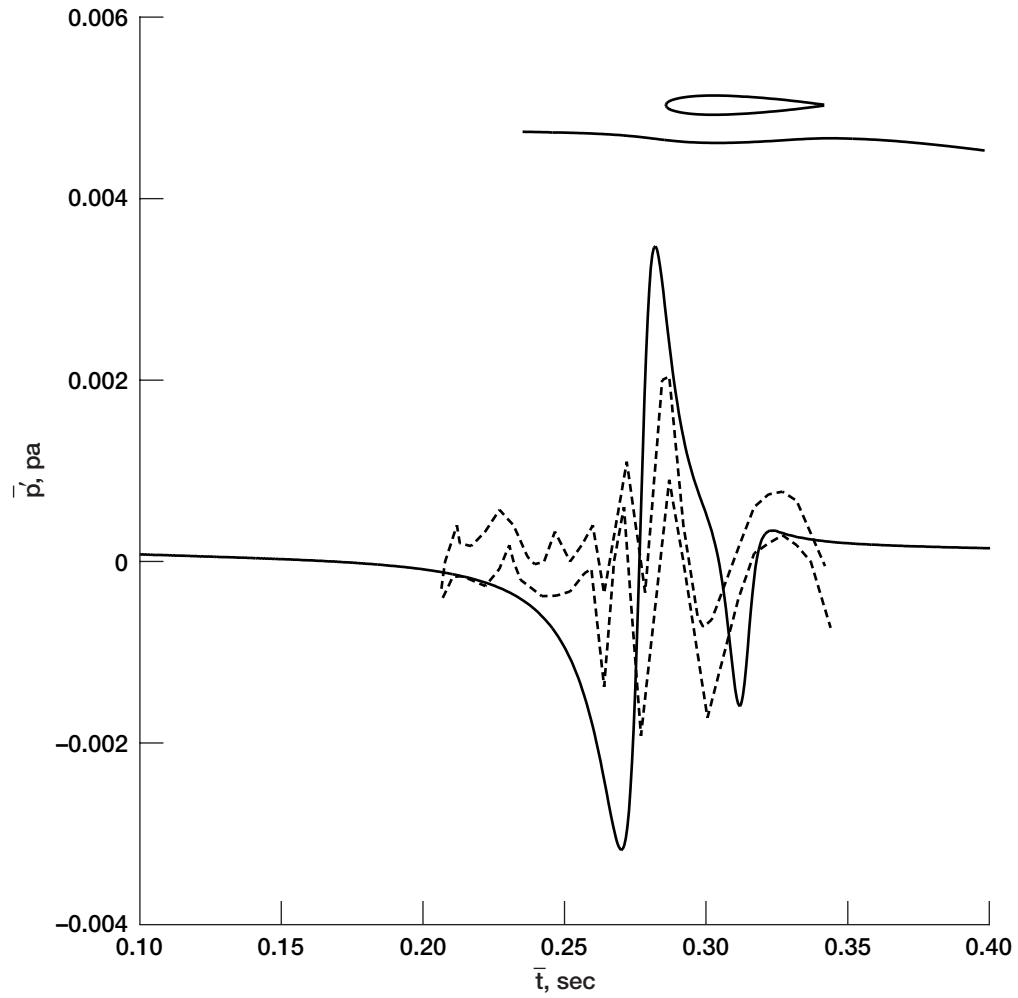


Figure 5.—Comparison of calculated acoustic pressure (the solid line) with Booth's experimental data. Observer's distance = 100 chord lengths; angle of attack = 0. Booth's test data of four different blade positions fall approximately in the area between two dashed lines.

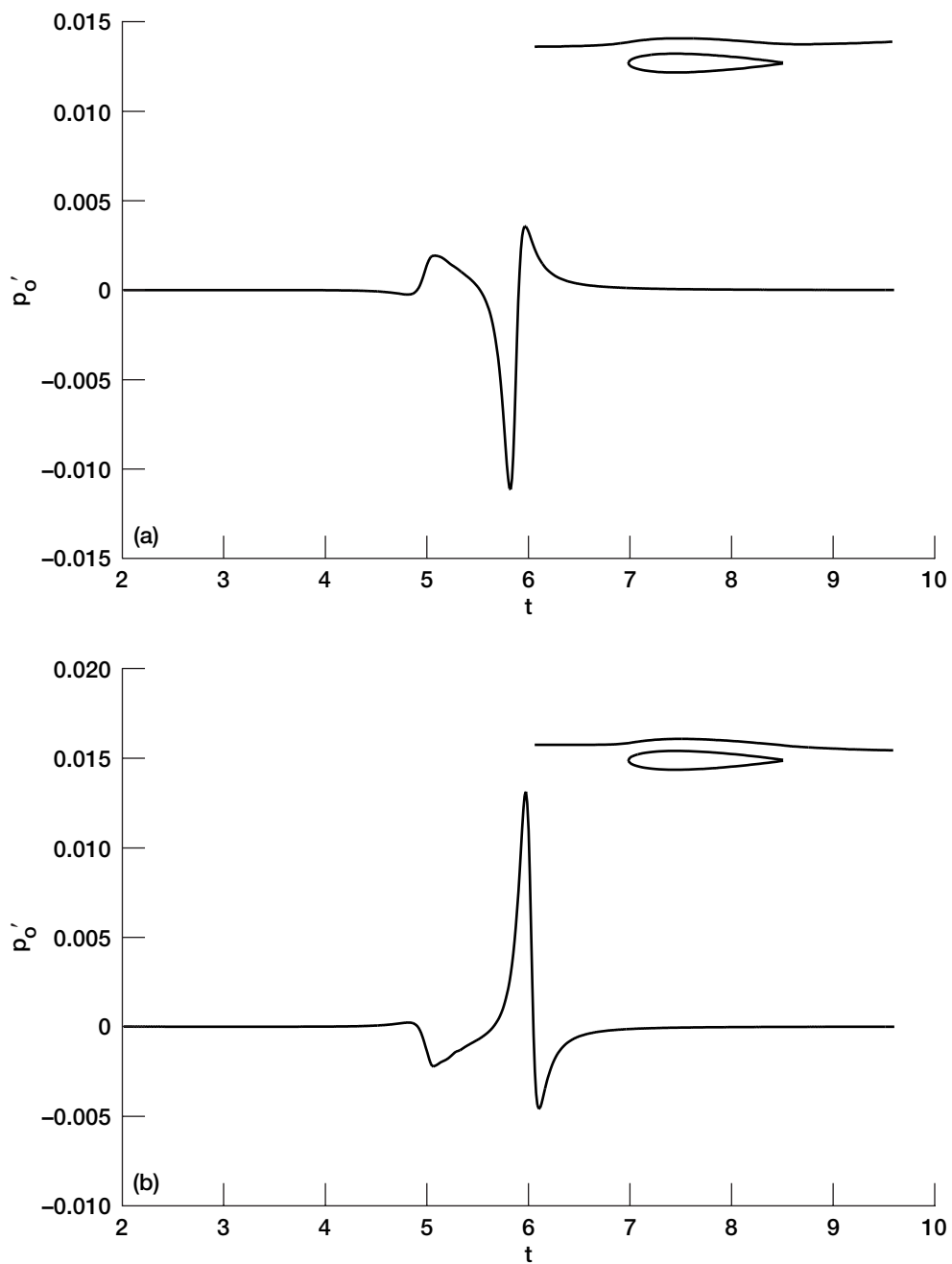


Figure 6.—Time history of sound generation by an NACA-0012 airfoil with a vortex passing above. $x_v = -5.0$, $y_v = 0.1$: (a) $\Gamma = -0.1$, (b) $\Gamma = 0.1$.

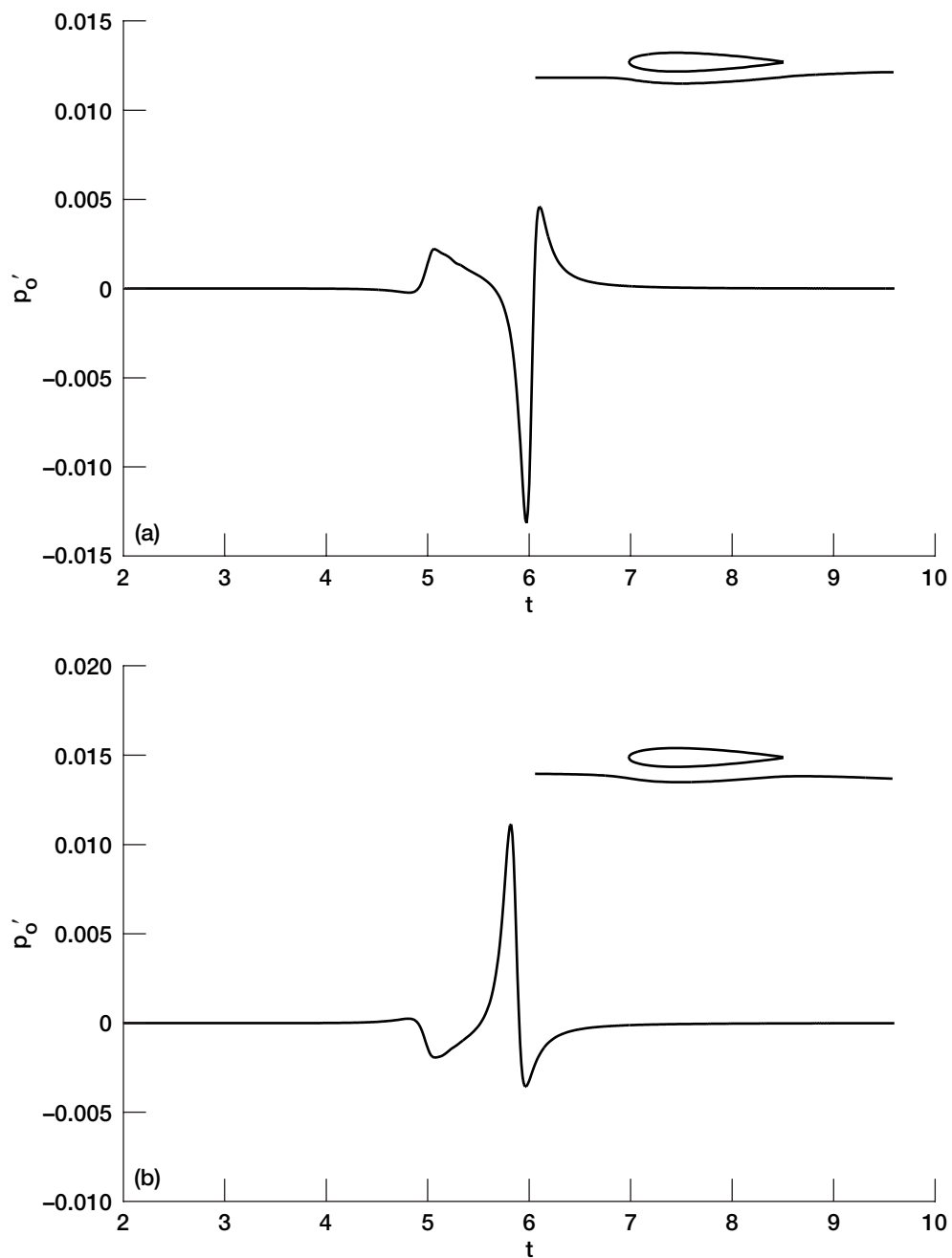
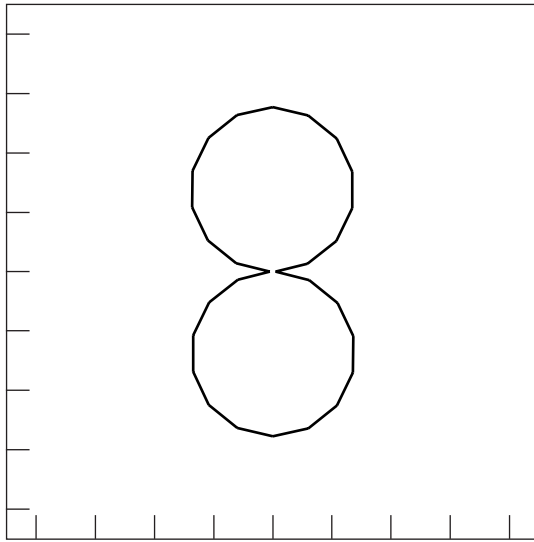
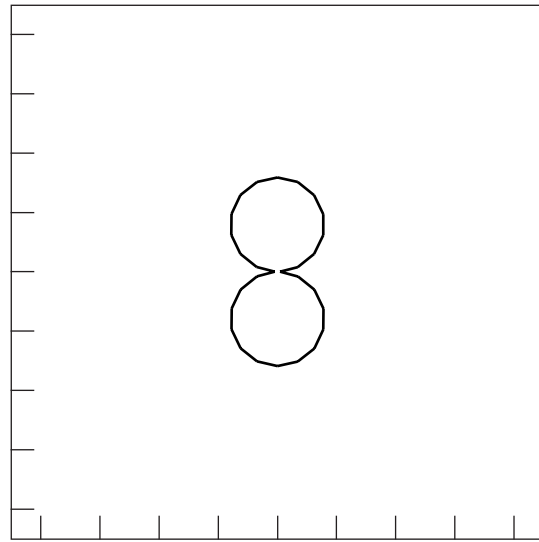


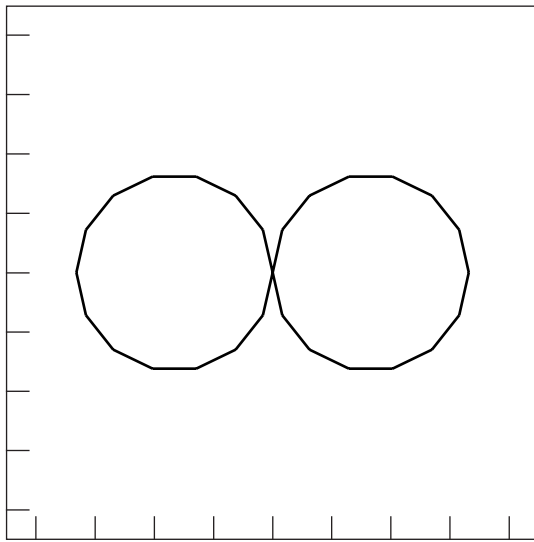
Figure 7.—Time history of sound generation by an NACA-0012 airfoil with a vortex passing below. $x_v = -5.0$, $y_v = -0.1$: (a) $\Gamma = -0.1$, (b) $\Gamma = 0.1$.



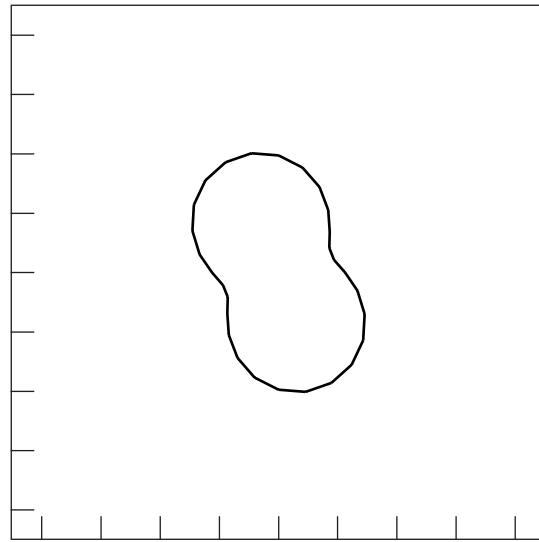
(a)



(b)



(c)



(d)

Figure 8.—Directivity for: (a) Fig. 6a; (b) Fig. 9b; (c) Fig. 12b; (d) Fig. 13a.

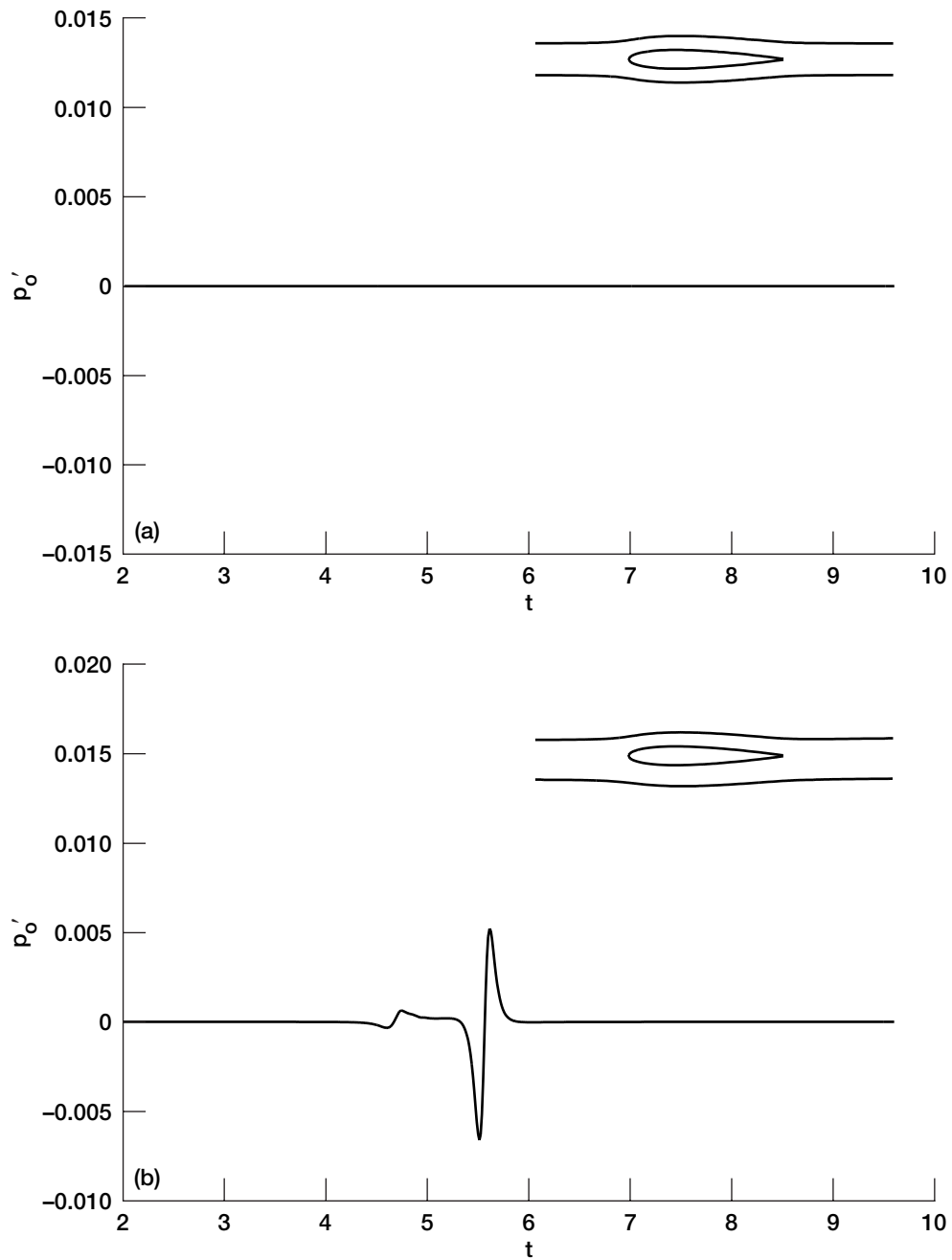


Figure 9.—Time history of acoustic interference. (a) Complete destruction: $\Gamma = -0.1$, $x_v = -5.0$, $y_v = 0.1$; $\Gamma = 0.1$, $x_v = -5.0$, $y_v = -0.1$. (b) Partial destruction: $\Gamma = -0.1$, $x_v = -5.0$, $y_v = 0.1$; $\Gamma = 0.1$, $x_v = -5.0$, $y_v = -0.15$.

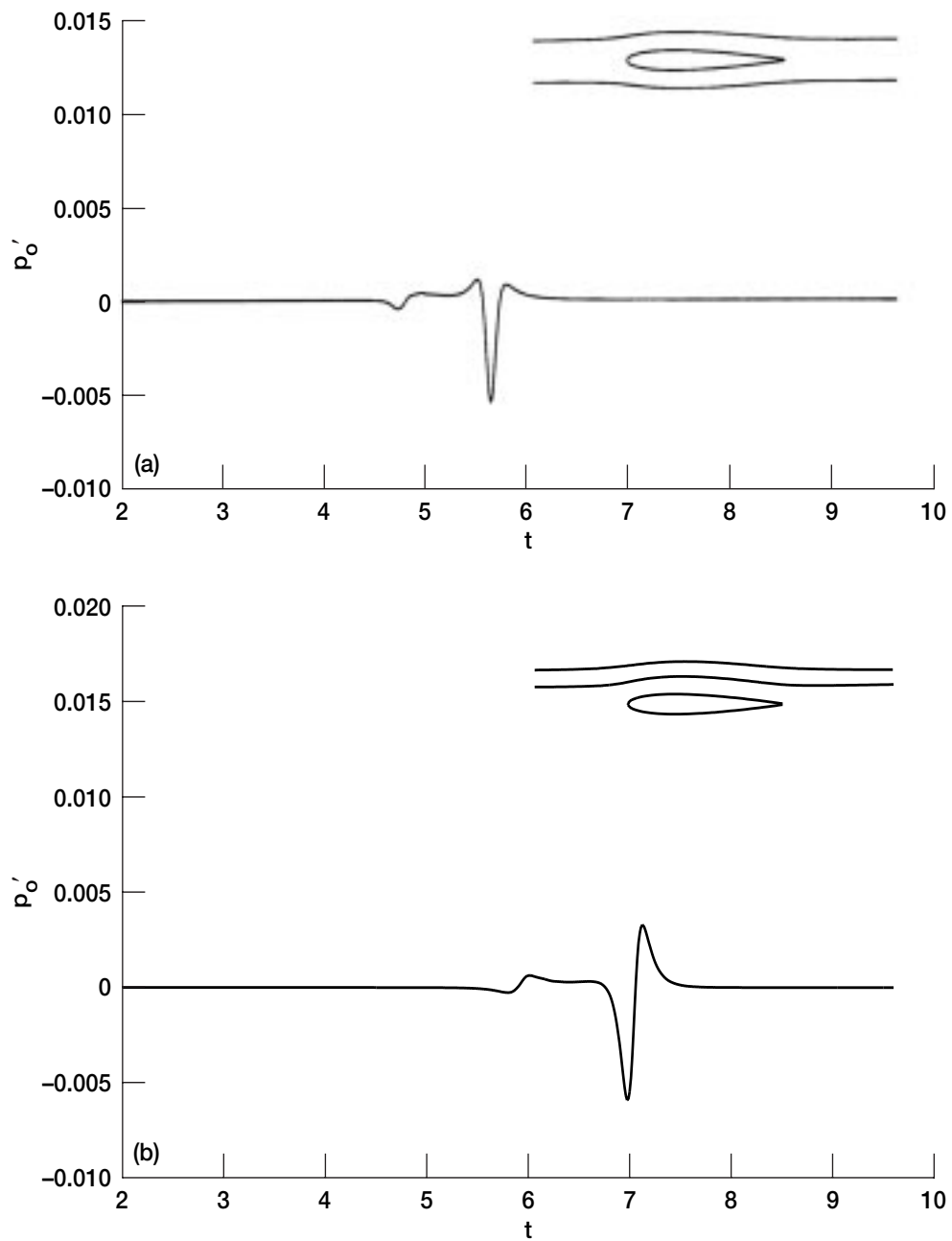


Figure 10.—Time history of acoustic interference. (a) Partial destructive interference: $\Gamma = -0.1$, $x_v = -5.0$, $y_v = 0.1$; $\Gamma = 0.085$, $x_v = -5.0$, $y_v = -0.15$. (b) Partial destructive interference: $\Gamma = -0.1$, $x_v = -5.0$, $y_v = 0.1$; $\Gamma = 0.1$, $x_v = -5.0$, $y_v = 0.2$.

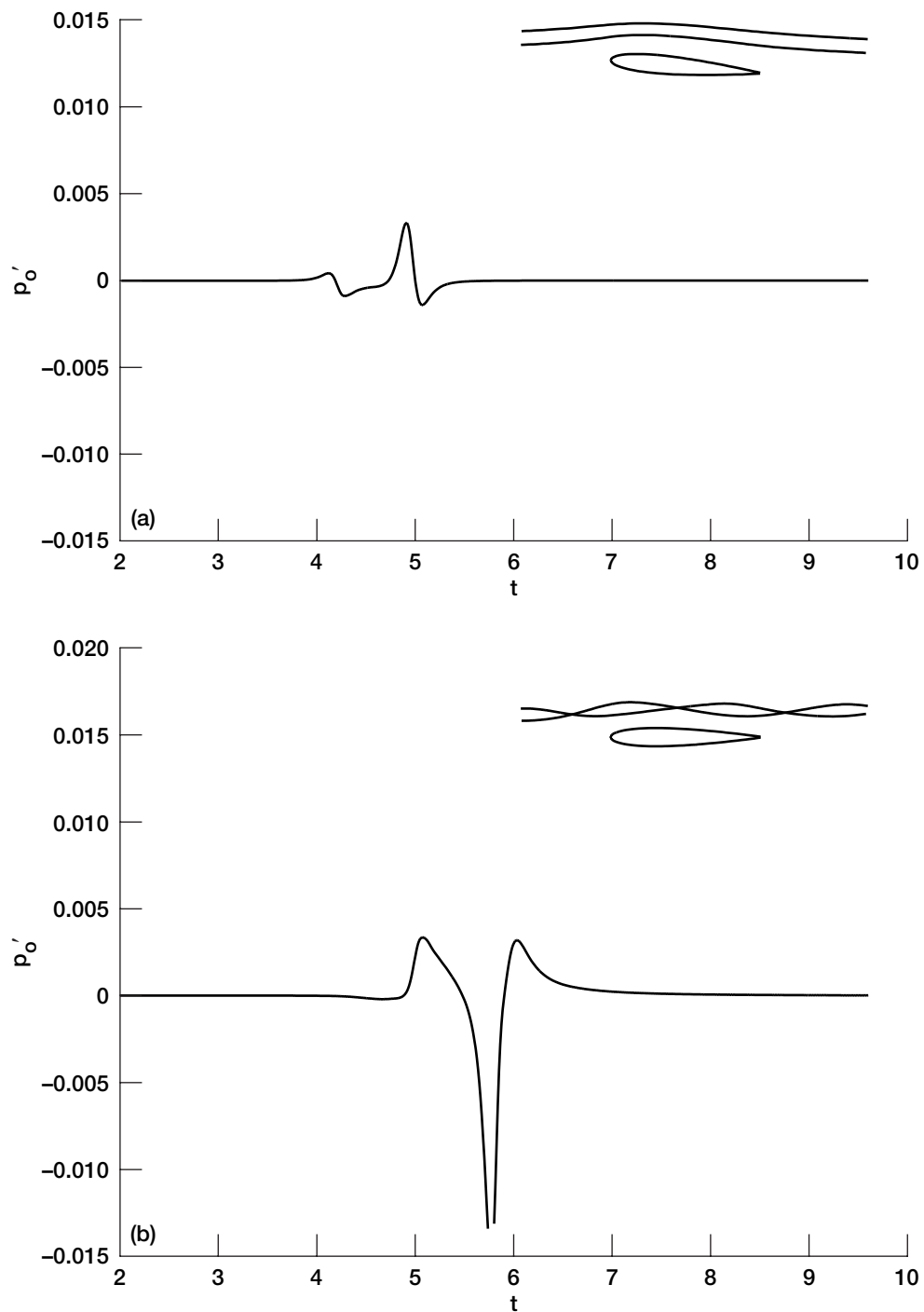


Figure 11.—Time history of acoustic interference. (a) Partial destructive interference with angle of attack = 5° : $\Gamma = 0.1$, $x_v = -5.0$, $y_v = 0.03$; $\Gamma = -0.1$, $x_v = -5.0$, $y_v = 0.12$. (b) Constructive interference: $\Gamma = -0.1$, $x_v = -5.0$, $y_v = 0.1$; $\Gamma = -0.1$, $x_v = -5.0$, $y_v = 0.18$.

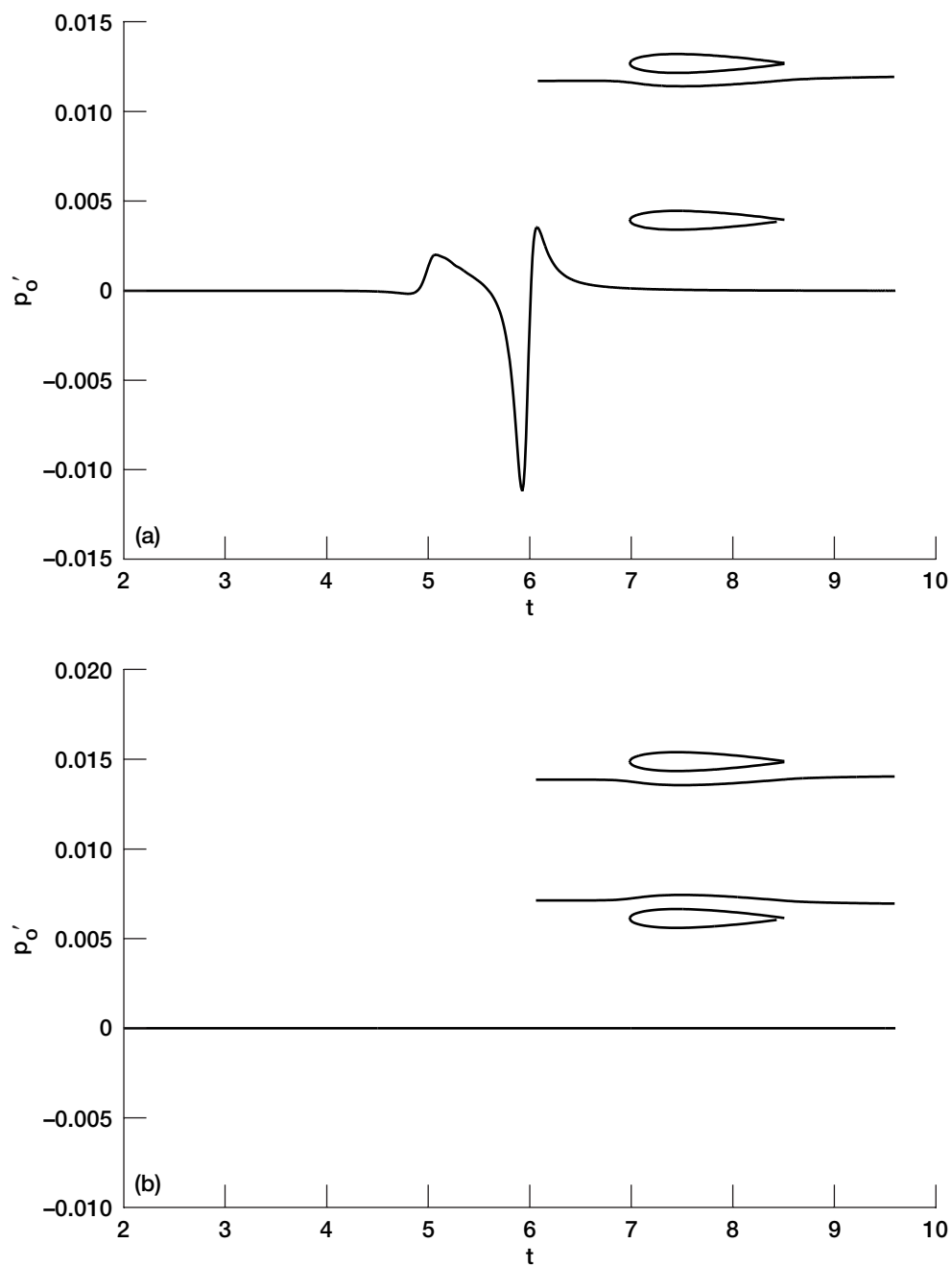


Figure 12.—Time history of sound generation by two stacked NACA-0012 blades.
 (a) One incident vortex; $\Gamma = -0.1$, $x_v = -5.0$, $y_v = -0.12$. (b) Two incident vortices;
 $\Gamma = -0.1$, $x_v = -5.0$, $y_v = -0.12$; $\Gamma = 0.1$, $x_v = -5.0$, $y_v = -0.88$.

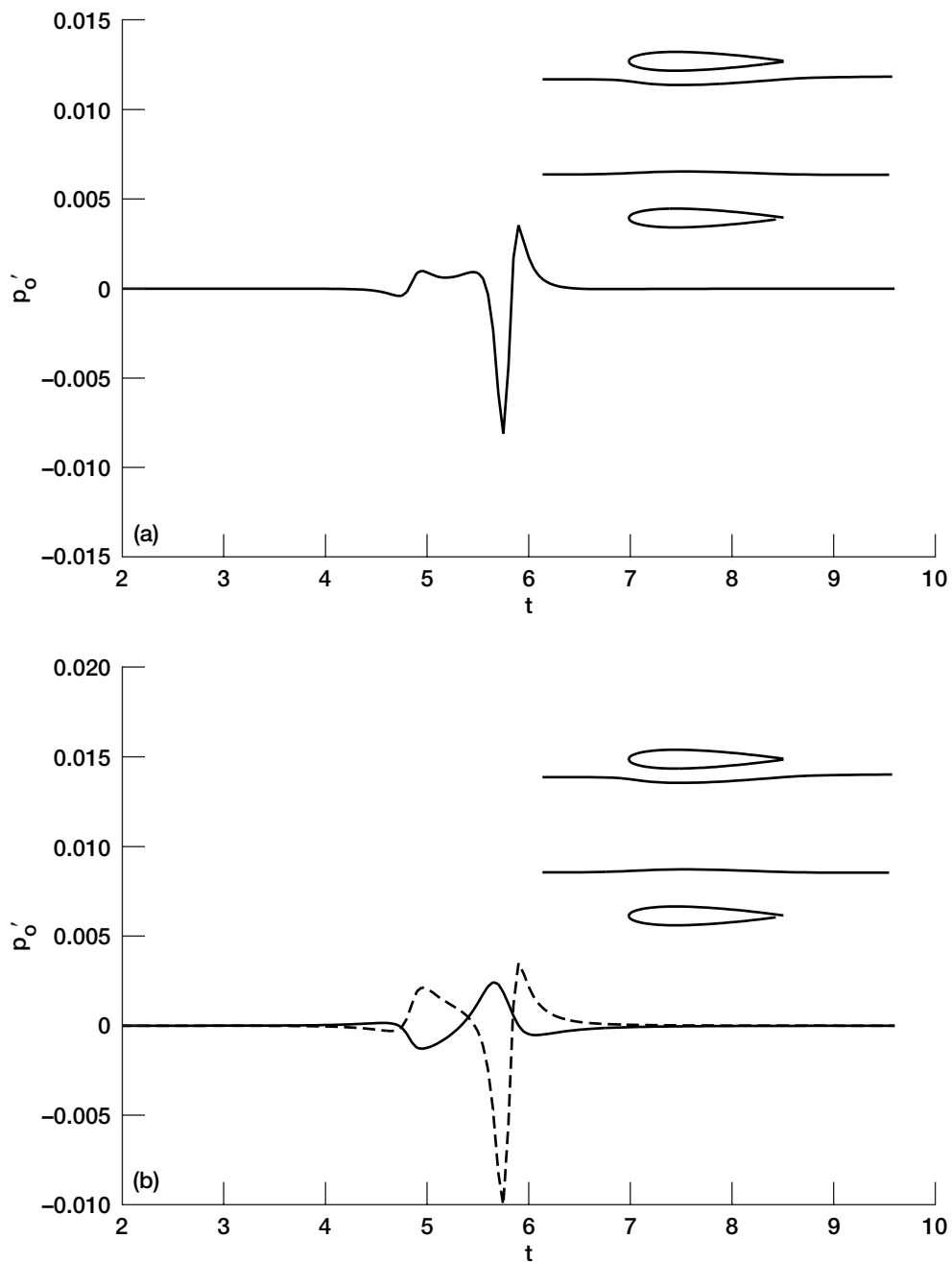


Figure 13.—Decomposition of acoustic pressure: $\Gamma = -0.1$, $x_v = -5.0$, $y_v = -0.12$; $\Gamma = 0.1$, $x_v = -5.0$, $y_v = -0.72$. (a) Acoustic pressure of the entire system. (b) —, acoustic pressure from the lower blade; ---, acoustic pressure from the upper blade.

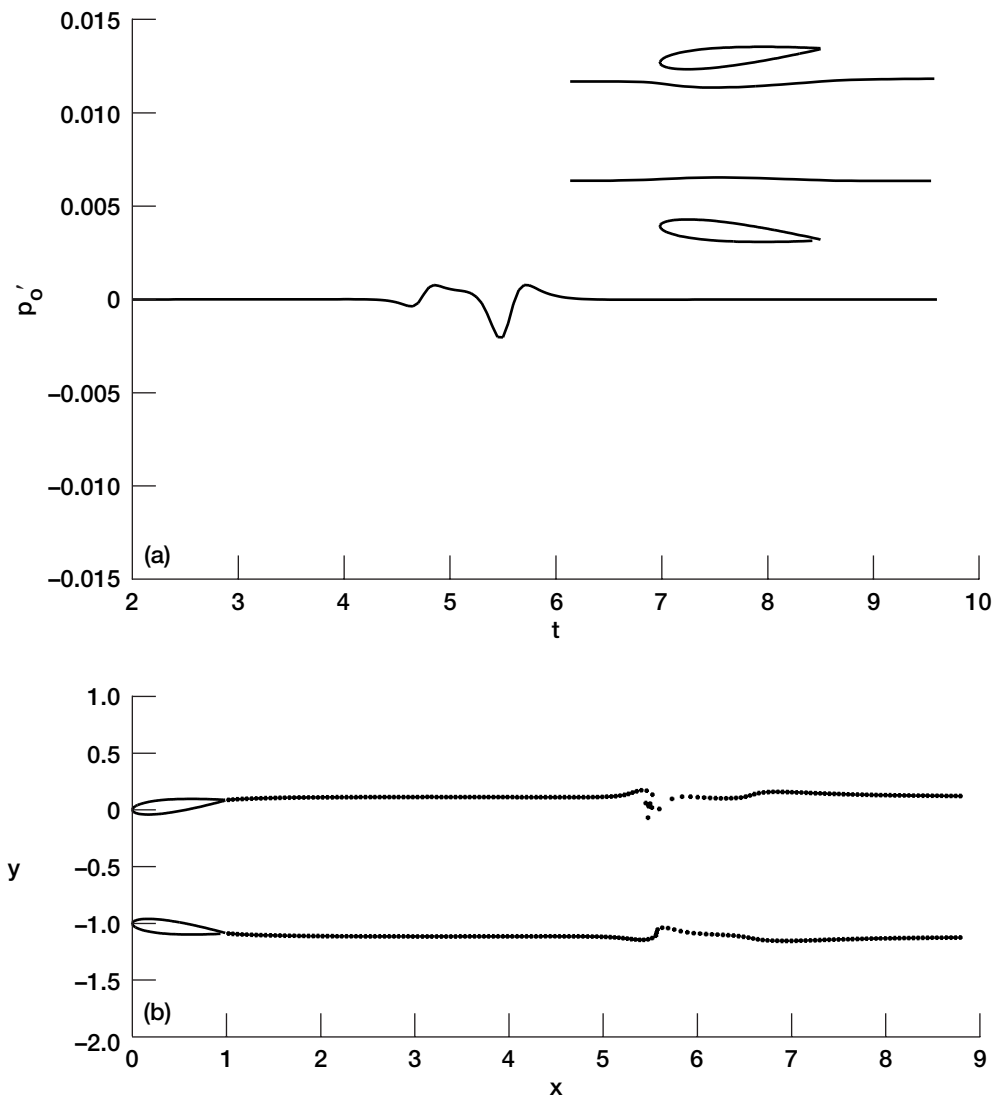


Figure 14.—Acoustic pressure and wakes: $\Gamma = -0.1$, $x_v = -5.0$, $y_v = -0.12$; $\Gamma = 0.1$, $x_v = -5.0$, $y_v = -0.72$. (a) Time history of acoustic pressure from two divergent NACA-0012 blades of 5° . (b) A snapshot of wakes.

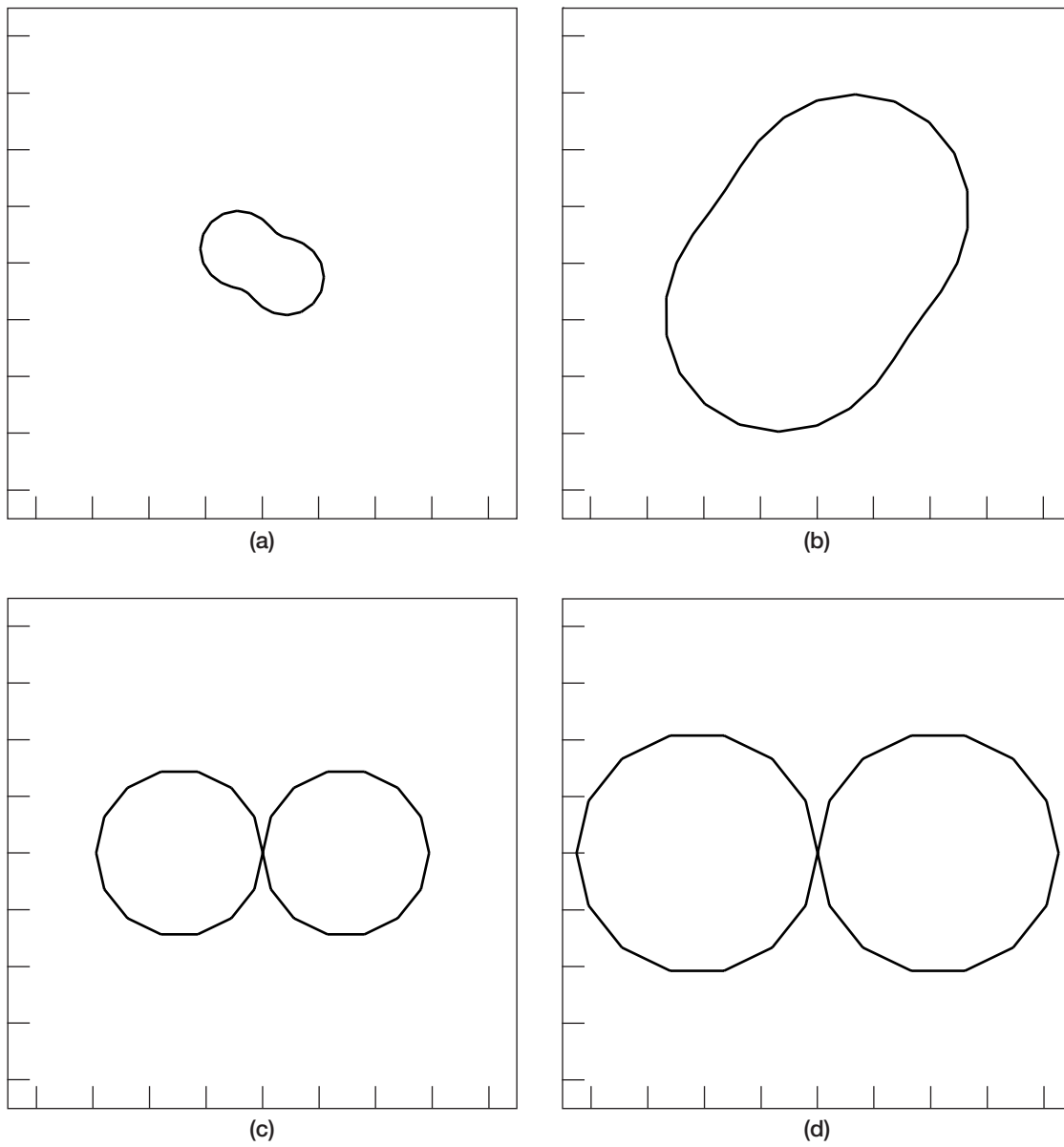


Figure 15.—Directivity for: (a) Fig. 14a; (b) Fig. 16a; (c) Fig. 16b; (d) Fig. 17a.

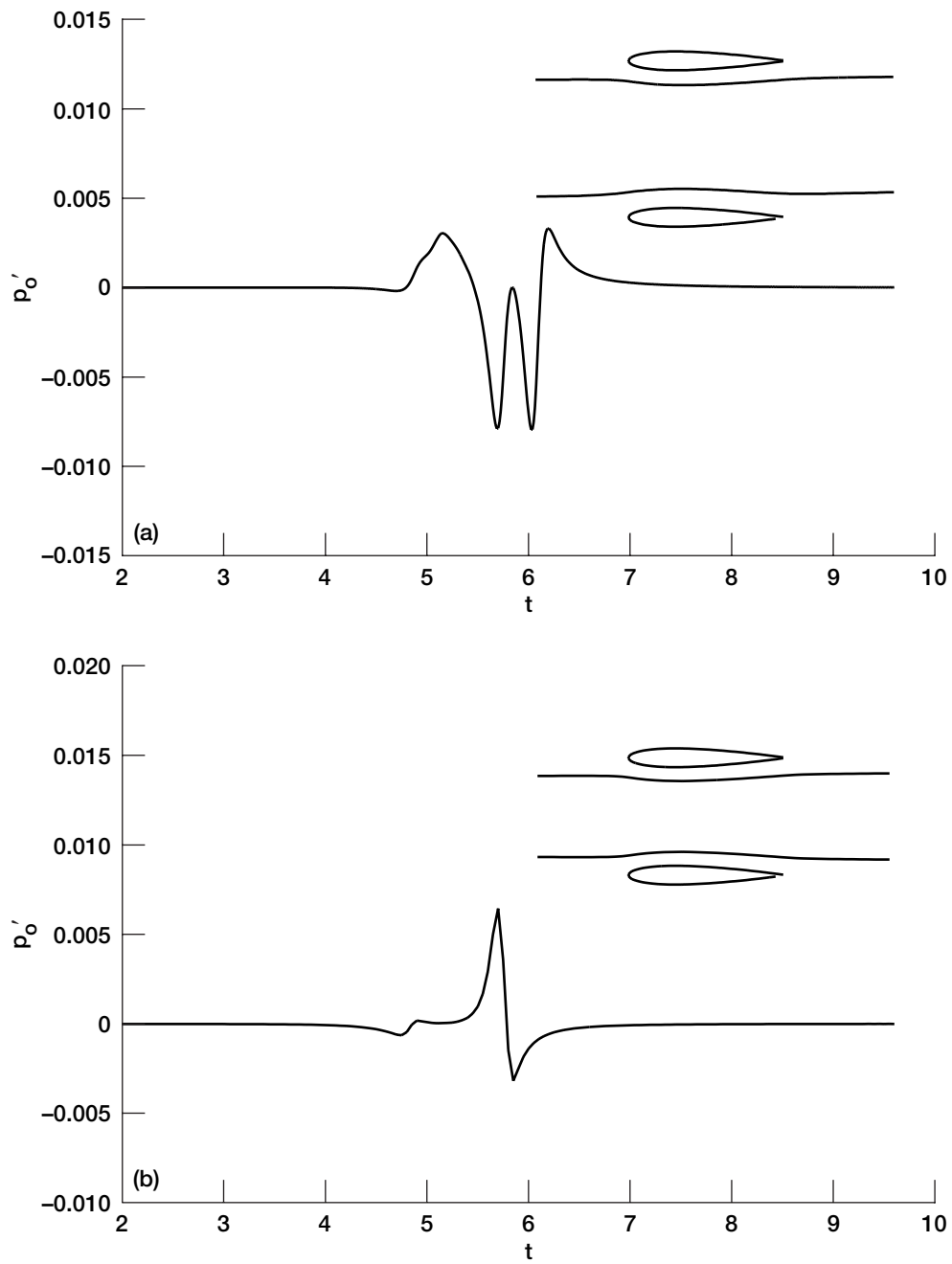


Figure 16.—Two examples of acoustic interference. (a) Two same-sense vortices: $\Gamma = -0.1$, $x_v = -5.0$, $y_v = -0.12$; $\Gamma = -0.1$, $x_v = -5.0$, $y_v = -0.88$. (b) Two opposite sense vortices; gap between blades = 0.75 chord lengths; observer's angle = 45° ; $\Gamma = -0.1$, $x_v = -5.0$, $y_v = -0.12$; $\Gamma = 0.1$, $x_v = -5.0$, $y_v = -0.63$.

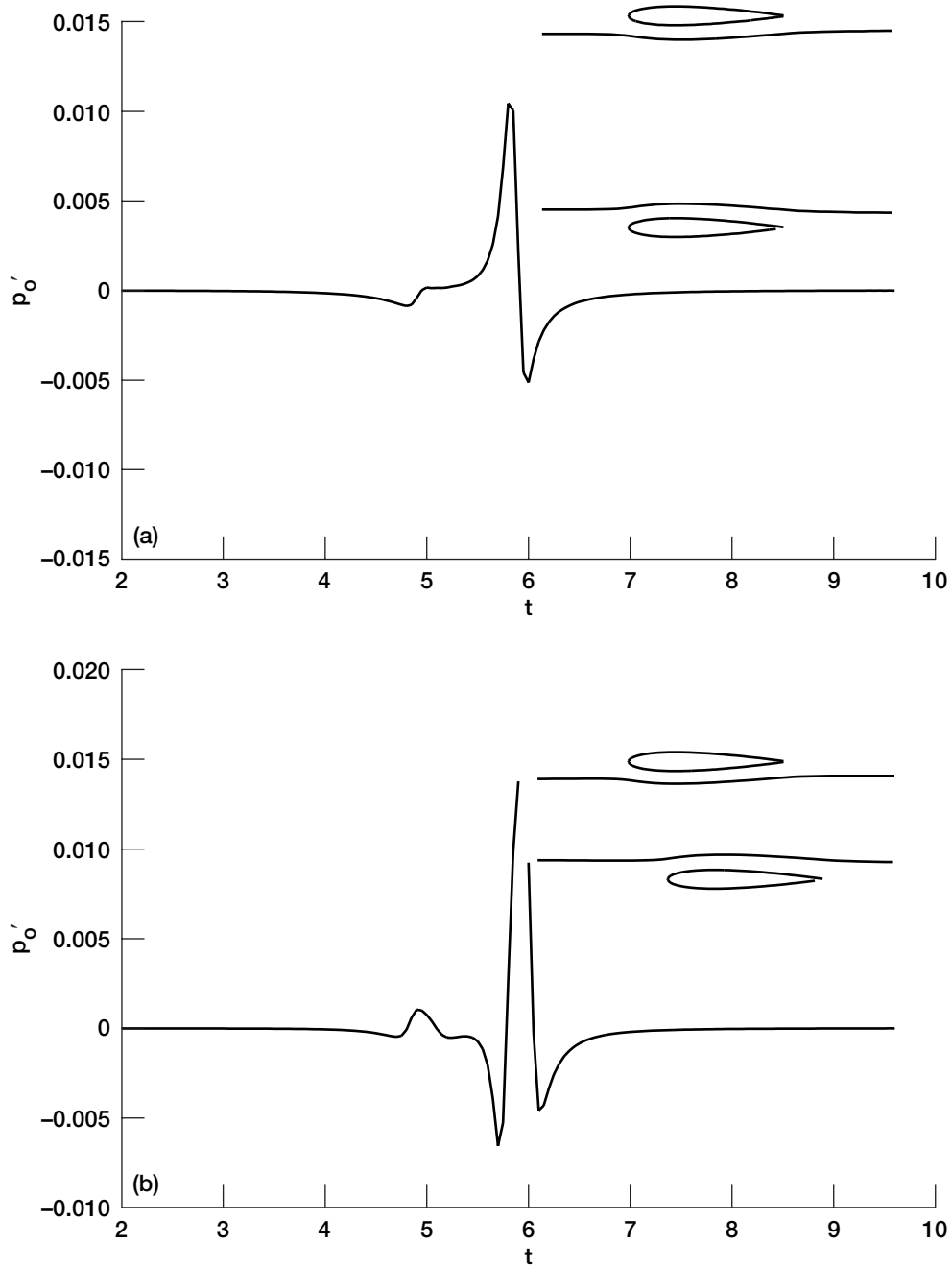
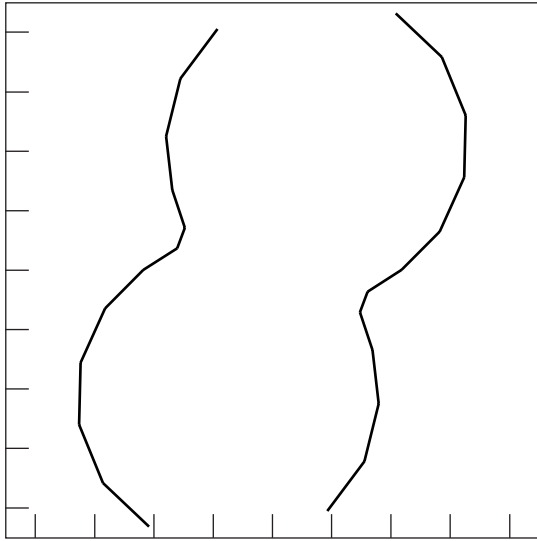
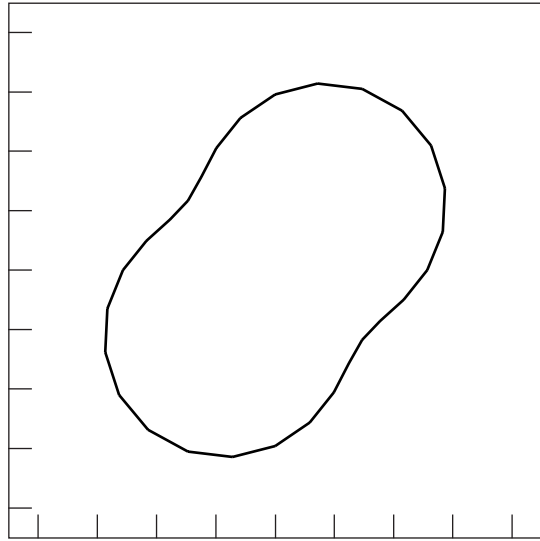


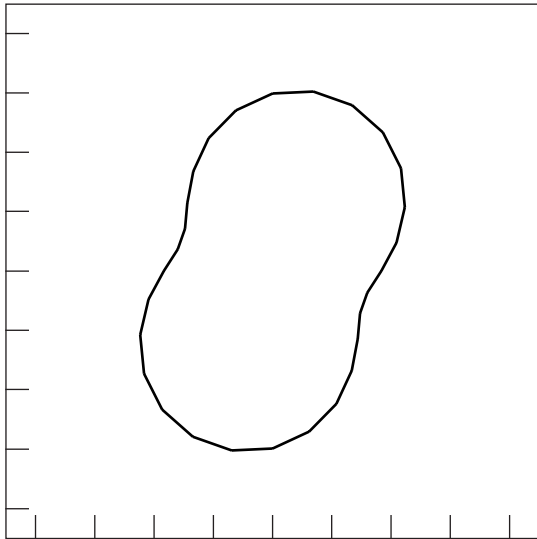
Figure 17.—Two additional examples of acoustic interference. (a) Conditions similar to Fig. 16b, except gap between blades = 1.35 chord lengths, and $y_v = -1.23$ instead of -0.63 . (b) Conditions identical to Fig. 16b, except that two blades are staggered.



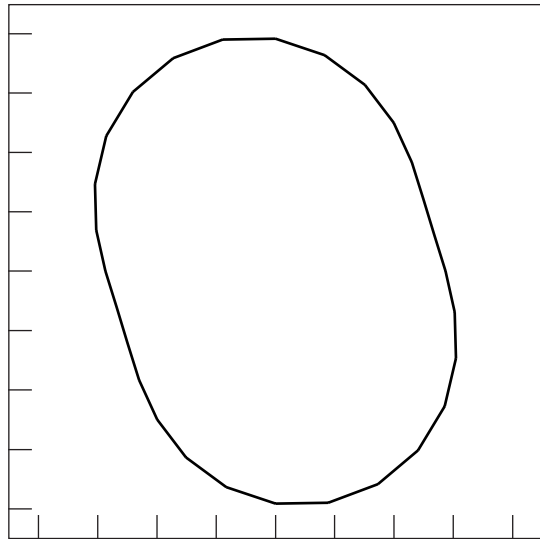
(a)



(b)



(c)



(d)

Figure 18.—Directivity for: (a) Fig. 17b; (b) Fig. 19a; (c) Fig. 20a; (d) Fig. 20b.

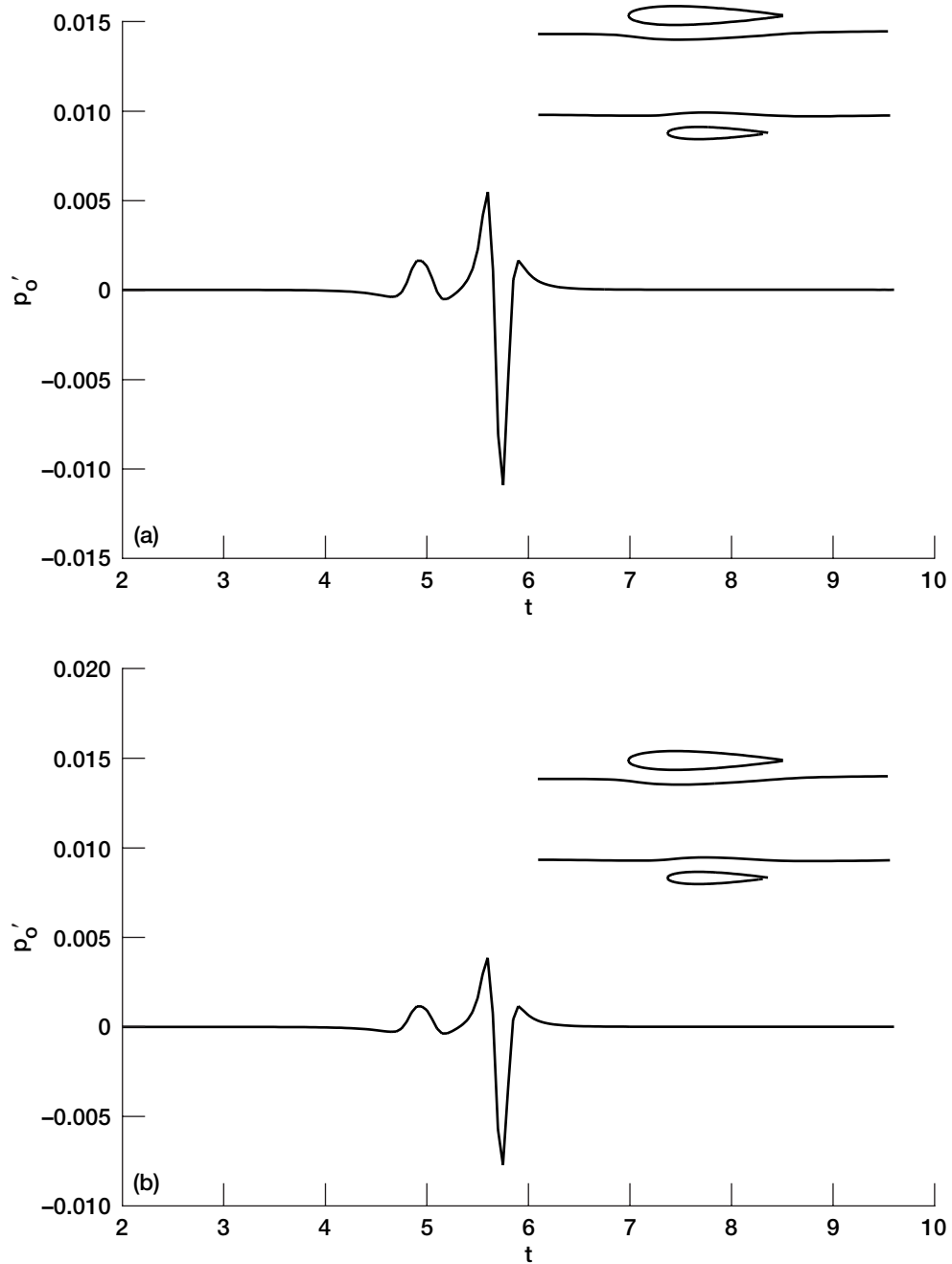


Figure 19.—Time history of acoustic pressure for two different observer's distances. (a) Two staggered blades with a smaller lower blade; observer's distance = 50 chord lengths; $\Gamma = -0.1$, $x_v = -5.0$, $y_v = -0.12$; $\Gamma = 0.1$, $x_v = -5.0$, $y_v = -0.63$. (b) Conditions identical to (a) except observed's distance = 100 chord lengths.

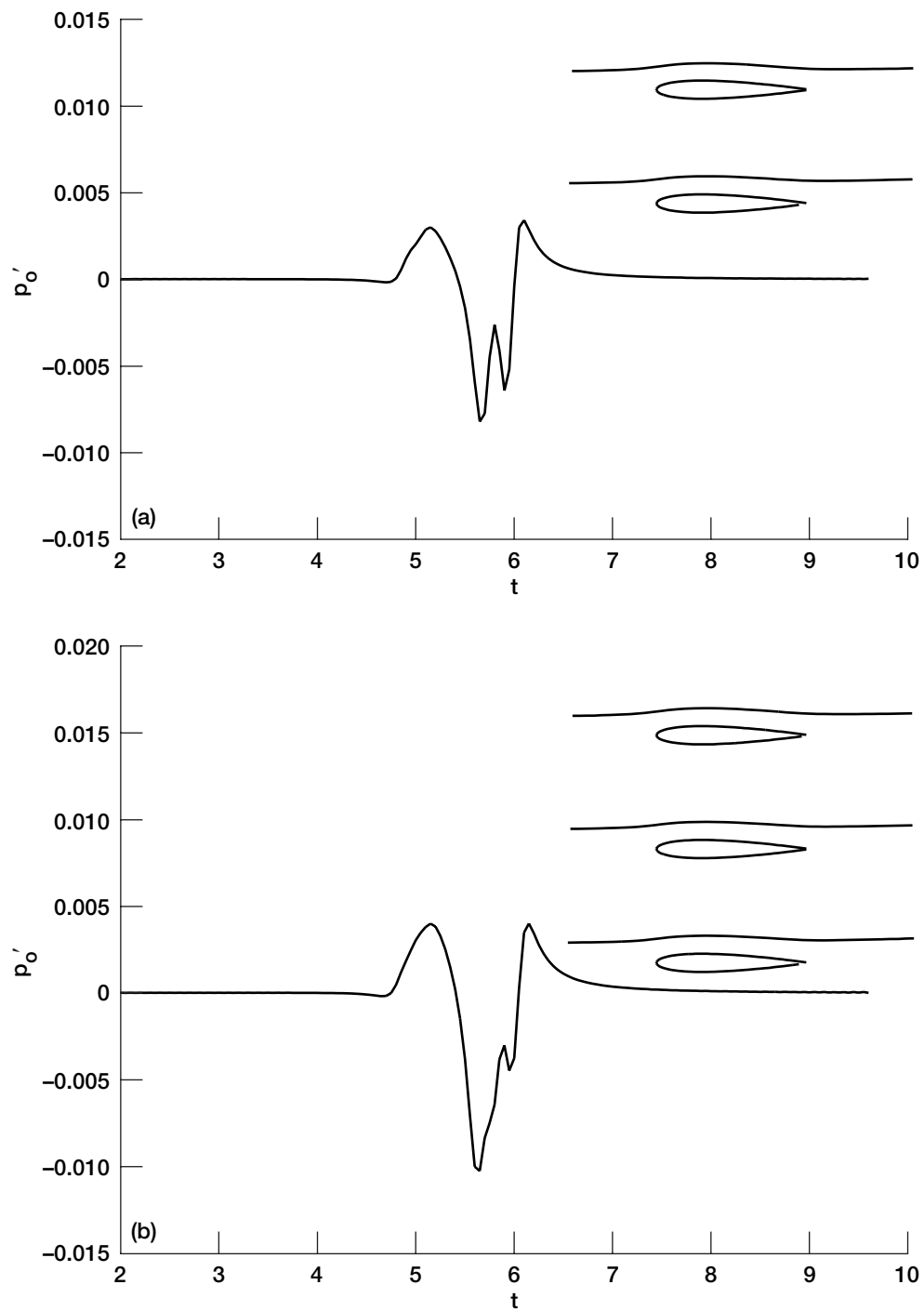


Figure 20.—Comparison of acoustic pressures between two and three stacked blades. (a) Gap between blades = 0.75 chord lengths; $\Gamma = -0.1$, $x_v = -5.0$, $y_v = 0.12$; $\Gamma = -0.1$, $x_v = -5.0$, $y_v = -0.63$. (b) Gap between blades = 0.75 chord lengths; $\Gamma = -0.1$, $x_v = -5.0$, $y_v = 0.12$; $\Gamma = -0.1$, $x_v = -5.0$, $y_v = -0.63$; $\Gamma = -0.1$, $x_v = -5.0$, $y_v = -0.87$.

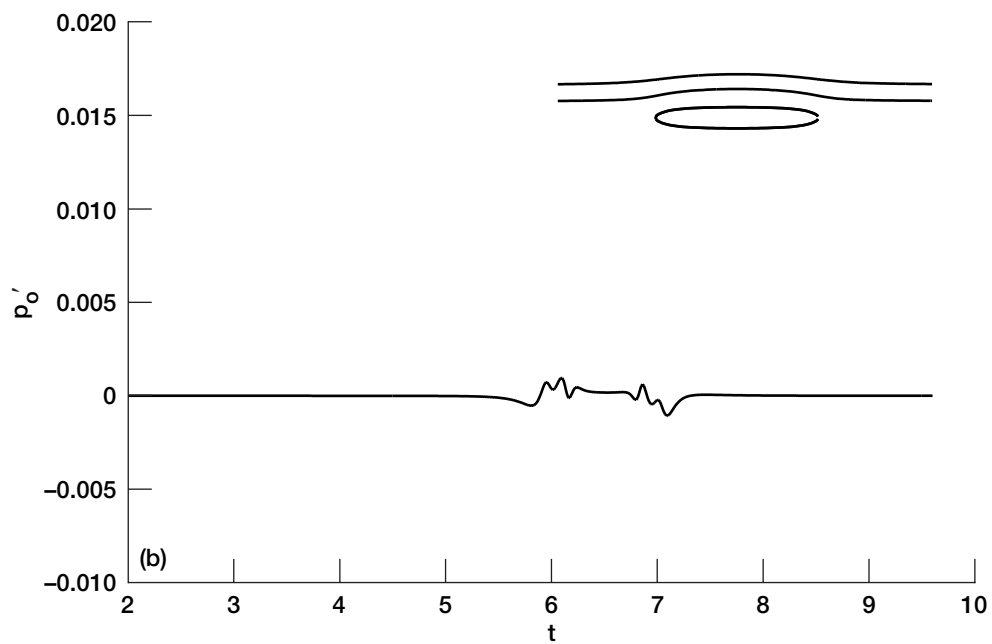
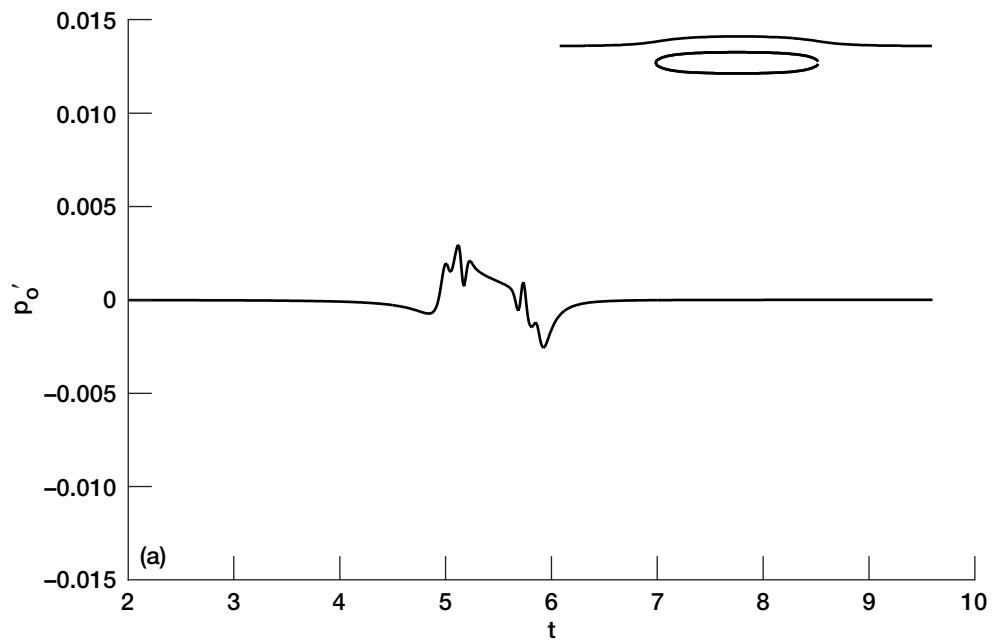


Figure 21.—Time history of acoustic pressure from non-lifting bodies. (a) $\Gamma = -0.1$, $x_v = -5.0$, $y_v = 0.1$. (b) $\Gamma = -0.1$, $x_v = -5.0$, $y_v = 0.1$; $\Gamma = 0.1$, $x_v = -5.0$, $y_v = 0.2$.

REPORT DOCUMENTATION PAGE			<i>Form Approved</i> <i>OMB No. 0704-0188</i>	
Public reporting burden for this collection of information is estimated to average 1 hour per response, including the time for reviewing instructions, searching existing data sources, gathering and maintaining the data needed, and completing and reviewing the collection of information. Send comments regarding this burden estimate or any other aspect of this collection of information, including suggestions for reducing this burden, to Washington Headquarters Services, Directorate for Information Operations and Reports, 1215 Jefferson Davis Highway, Suite 1204, Arlington, VA 22202-4302, and to the Office of Management and Budget, Paperwork Reduction Project (0704-0188), Washington, DC 20503.				
1. AGENCY USE ONLY (Leave blank)		2. REPORT DATE August 2000	3. REPORT TYPE AND DATES COVERED Technical Memorandum	
4. TITLE AND SUBTITLE Body-Vortex Interaction, Sound Generation and Destructive Interference			5. FUNDING NUMBERS WU-714-04-50-00	
6. AUTHOR(S) Hsiao C. Kao				
7. PERFORMING ORGANIZATION NAME(S) AND ADDRESS(ES) National Aeronautics and Space Administration John H. Glenn Research Center at Lewis Field Cleveland, Ohio 44135-3191			8. PERFORMING ORGANIZATION REPORT NUMBER E-12358	
9. SPONSORING/MONITORING AGENCY NAME(S) AND ADDRESS(ES) National Aeronautics and Space Administration Washington, DC 20546-0001			10. SPONSORING/MONITORING AGENCY REPORT NUMBER NASA TM-2000-210239	
11. SUPPLEMENTARY NOTES Responsible person, Hsiao C. Kao, organization code 5860, (216) 433-5866.				
12a. DISTRIBUTION/AVAILABILITY STATEMENT Unclassified - Unlimited Subject Category: 01 This publication is available from the NASA Center for AeroSpace Information, (301) 621-0390.			12b. DISTRIBUTION CODE Distribution: Nonstandard	
13. ABSTRACT (Maximum 200 words) It is generally recognized that interaction of vortices with downstream blades is a major source of noise production. To analyze this problem numerically, a two-dimensional model of inviscid flow together with the method of matched asymptotic expansions is proposed. The method of matched asymptotic expansions is used to match the inner region of incompressible flow to the outer region of compressible flow. Because of incompressibility, relatively simple numerical methods are available to treat multiple vortices and multiple bodies of arbitrary shape. Disturbances from vortices and bodies propagate outward as sound waves. Due to their interactions, either constructive or destructive interference may result. When it is destructive, the combined sound intensity can be reduced, sometimes substantially. In addition, an analytical solution to sound generation by the cascade-vortex interaction is given.				
14. SUBJECT TERMS Blade-vortex interaction; Asymptotic method; Aerodynamic noise; Noise reduction			15. NUMBER OF PAGES 47	
			16. PRICE CODE A03	
17. SECURITY CLASSIFICATION OF REPORT Unclassified	18. SECURITY CLASSIFICATION OF THIS PAGE Unclassified	19. SECURITY CLASSIFICATION OF ABSTRACT Unclassified	20. LIMITATION OF ABSTRACT	